AD-A144 751 THE EFFECTS OF RADIAL YARNS THREE-DIMENSIONALLY REINFORCED CARBON-CARBON..(U) CALIFORNIA UNIV LOS ANGELES SCHOOL OF ENGINEERING AND APPLIED.. 1/2

UNCLASSIFIED D QUAN ET AL. 01 JUL 84 UCLA-ENG-84-22 F/G 11/4 NL

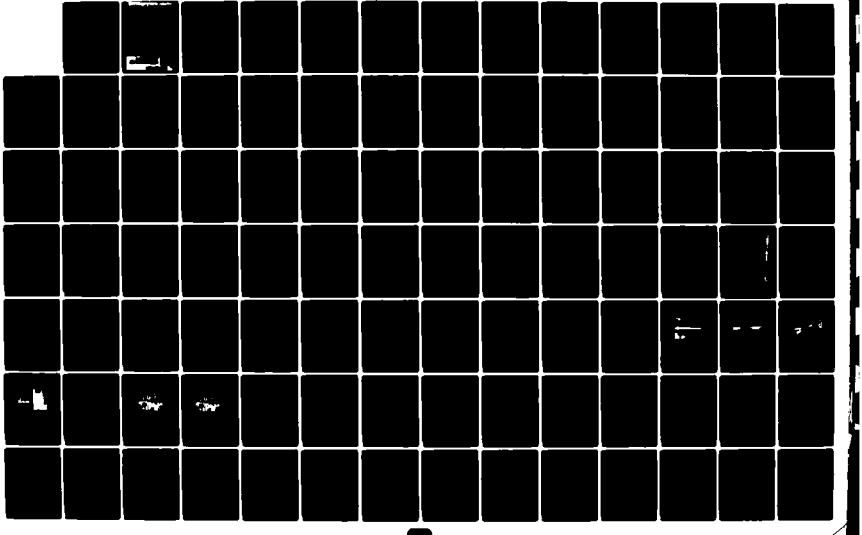

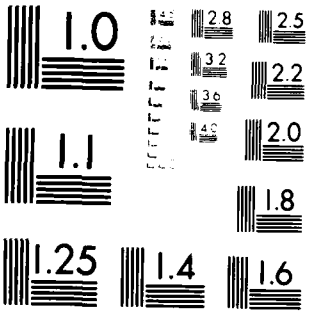

UCLA

AD-A1

THE EFFECTS OF RADIAL YARNS - THREEE-DIMENSIONALLY REINFORCED CARBON-CARBON COMPOSITES

by Douglas Quan, George Sines, S. B. Batdorf

ONR-N0014-77-C-0505
L. H. Peebles, Monitor

UCLA-ENG-81-22
JUNE 1981

Unclassified

SECURITY CLASSIFICATION OF THIS PAGE (When Data Entered)

(12)

REPORT DOCUMENTATION PAGE	READ INSTRUCTIONS BEFORE COMPLETING FORM
1 REPORT NUMBER	2 GOVT ACCESSION NO. AD-A144751 / 3 RECIPIENT'S CATALOG NUMBER
4 TITLE (and Subtitle) The Effects of Radial Yarns in Three-Dimensionally Reinforced Carbon-Carbon Composite	5 TYPE OF REPORT & PERIOD COVERED Technical Report
	6 PERFORMING ORG. REPORT NUMBER UCLA-ENG-84-22
7 AUTHOR(s) Douglas Quan, George Sines, S.B. Batdorf	8 CONTRACT OR GRANT NUMBER(s) N0014-77-C-0505
9 PERFORMING ORGANIZATION NAME AND ADDRESS School of Engineering and Applied Sciences University of California Los Angeles, CA 90024	10 PROGRAM ELEMENT, PROJECT, TASK AREA & WORK UNIT NUMBERS
11 CONTROLLING OFFICE NAME AND ADDRESS Office of Naval Research Att. Dr. A.M. Diness Arlington, Virginia 22217	12 REPORT DATE 1 July 84
	13 NUMBER OF PAGES 89
14 MONITORING AGENCY NAME & ADDRESS(if different from Controlling Office) Monitor, Dr. L.H. Peebles, Jr. Office of Naval Research Arlington, Virginia 22217	15 SECURITY CLASS. (of this report) Unclassified
	15a DECLASSIFICATION DOWNGRADING SCHEDULE

16 DISTRIBUTION STATEMENT (of this Report)

Unlimited

17 DISTRIBUTION STATEMENT (of the abstract entered in Block 20, if different from Report)

18 SUPPLEMENTARY NOTES

19 KEY WORDS (Continue on reverse side if necessary and identify by block number)

A

Carbon-Carbon Composites
Rocket Nozzles
Graphite
Fabrication Stresses

20 ABSTRACT (Continue on reverse side if necessary and identify by block number)

Some cylindrically wound, carbon-carbon billets have had gross fracture of the circumferential bundles during thermal processing. One function of the radial bundles is to reduce the stress that causes such fractures. An analysis is presented to show the potential reduction of the stress in the circumferential bundles during processing if the radial bundles remain

DD FORM 1 JAN 73 1473 EDITION OF 1 NOV 65 IS OBSOLETE
S/N 0102 LF 014 6601

SECURITY CLASSIFICATION OF THIS PAGE (When Data Entered)

intact. A simple analysis shows that the stress in the radial bundles is even higher than that in the circumferentials; therefore, they are likely to fail by either fracture or debonding. The radial bundles terminate at the outer and inner radii; an analysis is made of the debonding from the local shear near the ends of the radial bundles. Partial benefit of the radials might be obtained if creep reduced the stress in them. An experimental study on the creep of pitch-impregnated, uni-bundle specimens was conducted and results are presented. Based on creep of the radials, a procedure is presented to find an optimum time-temperature path to avoid failure of the radial bundles and characteristic optimum paths are presented. Exact optimum path shape cannot yet be proposed because the bond strength and bundle strength at elevated temperatures as well as the creep behavior are not yet known with sufficient accuracy.

The Effects of Radial Yarns,

Three Dimensionally Reinforced Carbon-Carbon Composite

Douglas Quan, George Sines, and S.B. Batdorf

Technical Report

for

Contract No. 0014-77-C-0505

Damage Mechanisms and Modeling of

Carbon-Carbon Composites

July 1984

Prepared for

Department of the Navy

Office of Naval Research

Arlington, Virginia 22217

REPORT ABSTRACT

Some cylindrically wound, carbon-carbon billets have had gross fracture of the circumferential bundles during thermal processing. One function of the radial bundles is to reduce the stress that causes such fractures. An analysis is presented to show the potential reduction of the stress in the circumferential bundles during processing if the radial bundles remain intact. A simple analysis shows that the stress in the radial bundles is even higher than that in the circumferentials; therefore, they are likely to fail by either fracture or debonding. The radial bundles terminate at the outer and inner radii; an analysis is made of the debonding from the local shear near the ends of the radial bundles. Partial benefit of the radials might be obtained if creep reduced the stress in them. An experimental study on the creep of pitch-impregnated, uni-bundle specimens was conducted and results are presented. Based on creep of the radials, a procedure is presented to find an optimum time-temperature path to avoid failure of the radial bundles and characteristic optimum paths are presented. Exact optimum path shape cannot yet be proposed because the bond strength and bundle strength at elevated temperatures as well as the creep behavior are not yet known with sufficient accuracy.

FORWARD

The text of this report consists of the masters thesis of Douglas Quan plus additional work presented in four addenda. The addenda are referenced in the body of the report. They give more detailed consideration of the uncertainty in the measurement in this study of the linear parameter of the creep equation, a discussion of the possible physical interpretation of the values measured for the activation energy for creep of carbon-carbon composites, analytical demonstrations of the effects that various creep and strength parameters would have on the optimum time-temperature path to avoid failure of the radial bundles, and some more detailed consideration of the stress in the radial bundles.

ABSTRACT OF THE THESIS

The Effects of Radial Yarns in

Three Dimensionally Reinforced Carbon-Carbon Composite

by

Douglas C. Quan

Master of Science in Engineering

University of California, Los Angeles, 1983

Professor George H. Sines, Chairman

Three-dimensional, cylindrically woven carbon/carbon composite is particularly appealing for rocket nozzle applications due to its favorable geometrical, thermomechanical and erosive properties. However, the performance of these materials is degraded by the presence of various kinds of in-process defects, such as pores, fiber buckles and cracks. The inhomogeneity and anisotropy of three-dimensionally woven carbon/carbon composite prevents accurate modeling of the material using classical elasticity; therefore elaborate computer codes for the finite element analysis are often employed. Although expensive to develop and employ, these programs are an indispensable tool for the analysis of three-dimensionally woven composites. However, analytical treatments using simple mathematics can provide a feeling for the physical state of the material which can be valuable to the designer. The intent of this work is to present one such analysis using a simplified approach.

Table of Contents

List of Figures & Tables

Nomenclature

C = circumfernce of billet

R = radius of billet

ϵ = strain

σ = stress

t = time

T = temperature

A = area

x = spacing

P = pressure

F = force

Subscripts

o = outer

i = inner

$\theta\theta$ = circumferential surface, circumferential direction

rr = radial plane, radial direction

zz = axial plane, axial direction

t = tension

c = compression

$\hat{a}$ = axial direction

$\hat{t}$ = transverse direction

f = fiber

m = matrix

1 = initial

Superscript

I,II,III,IV,... ,n = n^{th} iteration

M = mechanical

T = thermal

Introduction

While fracture of the circumferential yarn during heating in fabrication has received most of the attention, a simple analysis can show damage to the radial yarn is more likely because of its higher stress. The well-being of the radial fiber is very important to the integrity of the billet as a whole. When the billet is heated, the outer radius will be forced outward; the radial yarn wants to prevent this from happening by loading itself in tension, thereby relieving some of the load in the hoop yarns.

Unlike the hoop yarn, the radial yarn is not continuous. Both ends of the radial yarn intersect a free surface, thus a zone of high shear must be established at both ends of the yarn. If these shear stresses are greater than the yarn/matrix interface shear strength, the fiber bundle will tear away from the surrounding composite so that the only tensile stress in the bundle are those resulting from the frictional transfer between the yarn and the surrounding matrix. Sudden unloading, such as debonding of the radial yarn, could lead to catastrophic failure of the circumferential fiber bundle during processing; even gradual unloading can lead to degradation of the overall strength of the finished billet.

A careful crack study has been made by Kuhansedgh and Sines [1]. Some of the findings are summarized as follows:

(1) An extensive crack structure is seen in the circumferential surface*, which in some cases tends to be periodic; that is, cracks tend to occur after each five or six circumferential fiber bundles.

(2) There are a few cracks around some of the axial fibers but no extensive crack pattern is present around these fibers.

(3) Most radial fibers were totally surrounded by well-defined cracks. Although some appeared to have well-defined cracks on only three sides, the fourth side may also have been debonded and these cracks were continuous around the radial fiber throughout the billet, Fig.1.

Point (3) seems to support our claim that high stress in the radial fiber bundle, causes the debonding. This is because if the crack are caused only by shrinkage the distribution of crack should be quite even, since the shrinking of the matrix material is assumed to be isotropic. The striking contrast in the finding between the least stressed yarn, point (2) and the most severely stressed yarn

* Circumferential cracks are those in the surface perpendicular to the radial direction. The surface contains the circumferential and axial directions.

point (3) suggested that stress level in the fiber must play a role in crack formation.

It is the purpose of this study to take advantage of the creep process during the late graphitization cycles and develop a heating schedule so that fiber bundle debonding will be minimized, thereby preserving the integrity and minimizing micro-cracking which is not caused by shrinkage of the matrix.

The Billet and its Fabrication

The NAVY-C4X1 billet is a three-dimensional, cylindrically woven carbon/carbon composite. The billet is manufactured by General Electric, using multiple high pressure impregnation process at 15 ksi with CP277-15V coal tar pitch; which is supplied by the Allied Chemical Corporation. The billet is woven by two different kinds of yarns. HM-10000 yarn is used in the axial and circumferential directions, and the HM-3000 yarn in the radial direction. 10000 and 3000 corresponds to the number of filaments in each yarn; both yarns are fabricated by the Hercules Incorporated, Magnamite Graphite Fibers Division. The variable fiber volume fractions are shown in Fig.2, and the properties of the fiber and pitch materials are presented in Table (1) and Table (2).

Processing of the billet can be divided into two steps: Automatic weaving and densification. Fig.3 shows the process flow chart of the billet.

Automatic weaving of this three-dimensionally reinforced, carbon/carbon composite billet consisted of fabricating and assembly of yarn bundles of three orthogonal directions (radial, axial, circumferential). The billet is then heated to a minimum temperature of 350 C (662 F) before the densification process begins. In the densification process the billet was densified by subsequent impregnation,

carbonization, and graphitization steps using pitch materials as the impregnant. During the carbonization stage of the first cycle the matrix material became graphitizable carbon, forming mesophase during the heating treatment in the range from 400 C (750 F) to 450 C (840 F). Mesophase consists of large polycondensed aromatic compounds oriented nearly parallel to each other but still remaining in the liquid state.

Impregnation of carbon/carbon composite materials started after the first cycle of carbonization and graphitization in order to fill up the cracks which were generated during those steps. This step known as vacuum impregnation, was carried out at 240 C (480 F) under a pressure of 40 torr. The degree of impregnation depends upon the processing conditions such as pore size, pore size distribution, and gas permeability.

High pressure carbonization was the second stage of the densification process. The billet was heated to 650 C (1200 F) where the material carbonized; some cracking due to this phase change resulted in a relatively stress-free material at this step. The amount of cracking at this stage is observed to be small compared to cracking in subsequent steps.

The last step is graphitization, the billet was subjected to a uniform temperature rise up to 2750 C (5000 F). At this stage some chemical and structural changes occurred in the matrix. The densification process was repeated four times, the latter three in order to replace material volatilized during carbonization and graphitization as well as to fill the cracks occurring each time on cooling from graphitization. The billet was then subjected to inspection and machining.

I. Estimation of Stress in the Radial Bundle

The following analysis gives an estimation of the relative magnitude of the stress in the radial bundle to that of the circumferential bundle. For the purpose of simplicity we assumed that the circumferential stress at the outer and inner radius are equal and opposite.

$$(\sigma_{\theta\theta})_o = -(\sigma_{\theta\theta})_i = | \sigma_{\theta\theta} |$$

which implies that $(\epsilon_{\theta\theta})_o = -(\epsilon_{\theta\theta})_i = | \epsilon_{\theta\theta} |$ From studying the results obtained by [1] and [3], this found to be an acceptable approximation. We also assumed that the Young's modulus in the direction along the fiber's axis are equal for both radial and circumferential bundles so that $(E_{rr})_a = (E_{\theta\theta})_a = E$. Table (1) show that the difference in moduli between these two types of fiber bundles in the navy billet is about eight percent. Lastly the effect of the axial bundles were not considered in this analysis.

The circumference of the billet is $C = 2 \cdot \pi \cdot R$ When the billet is heated, the inner and outer circumferences of the billet will be forced to change its dimensions. The outer circumference just after a rapid heat up can be expressed as:

$$C_o' = C_o + \Delta C_o = C_o + C_o \epsilon + C_o \alpha \Delta T \qquad (I\text{-}1)$$

where ϵ is the mechanical strain.

$$2\pi R_o' = 2\pi R_o + 2\pi R_o \left[\frac{\sigma_{\theta\theta}}{E}\right] + 2\pi R_o \alpha\Delta T \tag{I-2}$$

$$R_o' = R_o \left[1 + \frac{\sigma_{\theta\theta}}{E} + \alpha\Delta T\right] \tag{I-3}$$

where α is the coefficient of thermal expansion, R is the original billet radius and R' is the billet radius just after a rapid heat up.

Similarly, the inner radius will be,

$$R_i' = R_i \left[1 - \frac{\sigma_{\theta\theta}}{E} + \alpha\Delta T\right] \tag{I-4}$$

The mechanical strain in the radial direction is

$$\epsilon_{rr} = \left[\frac{(R_o' - R_i') - (R_o - R_i)}{R_o - R_i}\right] - \alpha\Delta T \tag{I-5}$$

$$\epsilon_{rr} = \left[\frac{R_o + R_i}{R_o - R_i}\right] \frac{\sigma_{\theta\theta}}{E} \tag{I-6}$$

This is the maximum mechanical strain that a radial bundle will experience, if perfect bonding exists between the radial and the boundaries circumferential bundles. Stress in the radial bundle would be:

$$\sigma_{rr} = E_{rr}\,\epsilon_{rr} = E_{rr}\left[\frac{\sigma_{\theta\theta}}{E_{\theta\theta}}\right]\left[\frac{R_o + R_i}{R_o - R_i}\right] \tag{I-7}$$

Since we have assumed $E_{rr} = E_{\theta\theta}$ along the fiber's axis,

$$\sigma_{rr} = \sigma_{\theta\theta} \left[\frac{R_o + R_i}{R_o - R_i}\right] \qquad (I-8)^*$$

From the above analysis one can see that the stress in the radial bundles is always greater than that of the circumferential bundles. For a billet with short radial fiber or small $R_o - R_i$ relative to the billet circumference will result in very high radial stress, which agrees with physical intuition.

---

* Addendum IV further discusses the approximations made in this analysis. It also gives the results of a second-order approximate analysis made by Julius Jortner.

I-A The Restraining Effect of the Radial Bundle

The effect of the radial bundle on the billet's circumferential bundles can be demonstrated by modifying the computer model developed by Kuhansedgh and Sines [1]. In [1] the billet was modeled as an assembly of concentric thin walled cylinders. Alternate cylinders have different properties; one set models the fiber, the other the matrix. The number of cylinders modeling the fibers are equal to the number of layers of circumferential wrap. The Navy billet used in this study has 59 cylinders (numbered from 1 to 59). The odd numbers are for the fiber cylinders and the even numbers the matrix cylinders. Each cylinder can be expressed in a general form.

$$R_{(n,n+1)}(\alpha_f-\alpha_m)\Delta T = -\left[\frac{R_n^2}{t_n E_x}\right]P_{(n-1,n)} + (-1)^{n+1}\left[\frac{R_n^2}{t_n E_x} + \frac{R_{n+1}^2}{t_{n+1}E_y}\right]P_{(n,n+1)} - \left[\frac{R_{n+1}^2}{t_{n+1}E_y}\right]P_{(n+1,n+2)} \qquad \text{(IA-1)}$$

where n=1,2,3,... 59

When n = odd E_x = modulus of fiber

E_y = modulus of matrix

n = even E_x = modulus of matrix

E_y = modulus of fiber

The model also assumed that the properties of the fiber and the matrix cylinders will not change with temperature

and the concentric cylinders are initally in stress-free contact.

A change in temperature causes the cylinders' diameters to change, and thereby introduce inter-cylindrical pressure $P_{(n,n+1)}$ throughout the billet radii. These inter-cylindrical pressures can be obtained by solving a simultaneous set of equations which takes the form of equation (IA-1), these pressures can then be used to calculate the value of the billet's hoop fiber stress with the radial effect omitted Fig.4.

The restraining effect of the radial fiber can be modeled by applying a hydrostatic pressure at the inner and outer surfaces of the cylindrical walls. The magnitude of the hydrostatic pressure is equal to the traction induced by the highly stressed radial fiber on a characteristic area Fig.5. Stress on the radial fiber and its cross sectional area is assumed to be constant along its length, but the characteristic area decreases as you move towards the center of the billet; one should immediately realize that the hydrostatic pressure acting on the inner surface is greater than the pressure at the outer surface. Note that these hydrostatic pressures represent the restraining effect of the radial bundles on the hoop bundles, therefore we can only consider the amount of stress that has successfully transferred to the hoop bundle in calculating the

hydrostatic pressures. In this work the load transfer efficiency was assumed to be 0.50, it is a reasonable assumption considering the amount of debonding and cracks which is so commonly found around a fiber which intersects a free surface.

To calculate these restraining pressures the original billet model (with no radial effect) was utilized to find the stress of its hoop fibers. Knowing these stresses one can then calculate the change in billet radius just after a rapid temperature increase. Now a fictitious radial fiber is superimposed onto the billet with its ends fixed to the outer and inner most hoop fibers, one can then estimate the radial stress induced by the radius change. Recall, an assumption has been made that only 50% of the stress was successfully transferred and working to keep the billet from expanding, therefore the force in the radial bundle is multiply by a factor of 0.5. divide these force by their characteristic area and the results are the hydrostatic pressures. See appendix for detail mathematical illustrations.

The effect of these pressures can be seen by substituting them into the billet model. The results are plotted on Fig.6. This plot has over estimated the effectiveness of the radial bundle from a real billet. This is because the radial stress which was used to calculate the

hydrostatic pressures was computed from a billet where the maximum possible amount of expansion was allowed. In actual case internal frictional forces, anisotropy stresses and stuffing stresses will prevent the hoop fiber from expanding this much. Nevertheless the usefulness of a strong and well bonded radial fiber is reviewed. In this model, the presence of the radial fibers eliminated the entire compressive stress region and decreased the stress level of the outer portion of the billet by more then 20%. The sharp drops in stress level that you see in this plot is due to the model's extreme sensitivity to the variation of fiber volume fraction Fig.2.

In an actual billet a strong and well-bonded radial yarn is expected to help to reduce some of the processing anomalies. A smaller compressive zone can reduce mini-buckling at the inside diameter, lower tension at the outer diameter can reduce the chance of cracks formation in the rz plane. One would expect a flatter and smoother hoop stress distribution for the actual billet. In this analysis it was found that 58% of the hoop fibers have a stress value 1/3 of that in the radial fibers and 42% of the the hoop fibers have a stress value 1/2 of that in the radial fibers. These figures again reinforced our claim that the radial yarn is the most highly stressed bundles in the billet and its well-being is crucial to the integrity of the billet as a whole.

II. Fiber/Matrix Displacement Mismatch Analysis

Property mismatch between the fiber and matrix causing thermal stresses could lead to the ultimate failure of the cylindrically woven carbon/carbon composites during fabrication. Adhesive failure at the radial fiber or failure of the fiber itself is expected to take place before any other mode of failure. This is because the radial yarns are the most highly stressed, and regions of high shear stress are created at the free ends because of property mismatch.

Imagine a billet composed of equally spaced fibers with matrix in between, as shown in Fig.7. When heated, the fibers and matrix will expand, but the matrix will try to expand more because of its higher coefficient of expansion.

This mismatch will result in high shear stress at the fibers' ends. If the stress level exceeded the bond strength of the interface, debonding will initiate. Using some physical intuition, one can realize that the debonded portion of the matrix will try to flatten itself out, which translates into creating a pulling force on the matrix around the matrix-fiber interface Fig.8. If this situation were to occur, the usefulness of the radial yarn in terms of load carrying capacity is reduced by the debonding.

The fiber-matrix displacement mismatch can be analyzed, utilizing a model very similar to the one discussed earlier

in this section, Fig.7.

Balance of force exist between the fiber and the matrix during the heating up process is expressed by,

$$A_f E_f \epsilon_f^M = A_m E_m \epsilon_m^M \qquad \text{(II-1)}$$

The difference in mechanical strain is induced by the mismatch in coefficient of expansion:

$$\epsilon_f^M - \epsilon_m^M = (\alpha - \alpha_F)(T - T_1) \qquad \text{(II-2)}$$

where T_1 is the initial temperature

Let S be the shear force between the interacting surfaces, and has a dimension of force per unit length.

$$S = k_1 (U_f - U_m) \qquad \text{(II-3)}$$

where k_1 is a constant and U is displacement.

The same shear force can be written in terms of displacement of the fiber, or displacement of the matrix, which results from their respective strain.

$$S = \frac{d(A_f E_f \frac{dU_f^M}{dx})}{dx} \qquad \text{(II-4)}$$

If A_f and E_f are constant,

$$S = A_f E_f \frac{d^2 U_f^M}{dx^2} \qquad (II-5)$$

so that

$$\frac{d^2 U_f^M}{dx^2} = \frac{S}{A_f E_f} \qquad (II-6)$$

At the interface, the shear force acting on the fiber is equal but opposite in magnitude to the shear force acting on the matrix,

$$\frac{d^2 U_m^M}{dx^2} = -\frac{S}{A_m E_m} \qquad (II-7)$$

The difference in strain is:

$$\frac{d^2 (U_m - U_f)^M}{dx^2} = \left(\frac{1}{A_f E_f} + \frac{1}{A_m E_m}\right) k_1 \left[(U_m^M - U_f^M) + (U_m^T - U_f^T)\right] \qquad (II-8)$$

Since the thermally induced displacement is constant along the length of the fiber, we can rewrite equation (II-8) as:

$$\frac{d^2 (U_m - U_f)^M + (U_m - U_f)^T}{dx^2} = \left(\frac{1}{A_f E_f} + \frac{1}{A_m E_m}\right) k_1 \left[U_m^M - U_f^M + (U_m^T - U_f^T)\right] \qquad (II-9)$$

Let $(U_m - U_f)^M + (U_m - U_f)^T$ be D, the total displacement mismatch and $\left(\frac{1}{A_f E_f} + \frac{1}{A_m E_m}\right) k_1$ be a constant K^2. Then we get a differential equation of the form,

$$\frac{d^2D}{dx^2} - K^2D = 0 \tag{II-10}$$

The characteristic equation is $\lambda^2-K^2=0$, which can be factored into $(\lambda-K)(\lambda+K) = 0$. The roots are $\lambda_1=K$ $\lambda_2=-K$. Since the roots are real and distinct, the solution is

$$D = c_1e^{Kx} + c_2e^{-Kx} \tag{II-11}$$

For K=-K we can write

$$D = k_1\cosh Kx + k_2\sinh Kx \tag{II-12}$$

$$k_1 = c_1+c_2 \quad k_2 = c_1-c_2 \tag{II-13}$$

In obtaining the above solution, we use

$$\cosh Kx = \frac{1}{2}(e^{Kx}+e^{-Kx}) \tag{II-14}$$

$$\sinh Kx = \frac{1}{2}(e^{Kx}-e^{-Kx}) \tag{II-15}$$

The boundary conditions are:

$$U(0) = 0$$

and

$$U'(\frac{L}{2}) = \frac{d}{dx}(U_m^M-U_f^M) = (\alpha_m-\alpha_f)\Delta T \tag{II-16}$$

for U(0)=0

$$0=c_1+c_2 \qquad c_1=-c_2$$

for $U'(\frac{L}{2})=(\alpha_m-\alpha_f)\Delta T$

$$(\alpha_m-\alpha_f)\Delta T = c_1 K e^{Kx} - c_2 K e^{-Kx} \tag{II-17}$$

$$= c_1 K (e^{Kx}+e^{-Kx})$$

$$= 2c_1 K \cosh Kx$$

$$c_1 = \frac{(\alpha_m-\alpha_f)\Delta T}{2K} \cosh Kx \tag{II-18}$$

$$D = C_1 (e^{Kx}-e^{-Kx})$$

$$= c_1 2 \sinh Kx$$

$$D = \frac{(\alpha_m-\alpha_f)\Delta T \sinh Kx}{K \cosh Kx} = \frac{(\alpha_m-\alpha_f)\Delta T}{K} \operatorname{Tanh} Kx \tag{II-19}$$

Note that the total displacement mismatch, D is zero at the center and is maximum at the ends, equation (II-19). Large mismatch means great shear stress at the ends, which encourages the initiation of adhesive failure.

III. Critical Tensile Stress

In the previous section, it was shown that the property mismatch between the fiber and the matrix creates a displacement mismatch. For the following analysis everything surrounding a radial fiber will be considered matrix. This assumption can be argued by looking at an unit cell of the material, Fig.9. The elastic modulus of the axial and circumferential fibers are low along the radial direction. At elevated temperature, the transverse modulus of the fibers are very close to that of the matrix, reference [4]. In the light of this approximation, the assumption that the radial fiber is completely surrounded by matrix for stress analysis of the radial fiber along the radial direction will be valid.

The shear stress induced by the displacement mismatch caused by the difference in thermal expansion coefficient is analogous to the shear stress induced by displacement mismatch caused by the difference in elastic modulus. The latter problem has been treated by Cox, [5], using the so called "shear lag analysis". In this model a mechanical stress is applied on the infinite resin parallel to the embedded yarn. In the region of the yarn ends the strain of the fiber will be less than the average strain in the matrix. The deformation field in the matrix has been sketched in Fig.10. Cox shown that the tensile stress along

this yarn is given by:

$$\sigma_f = E_f \epsilon_m \left\{ \frac{1-\cosh \beta(\frac{1}{2}d-x)}{\cosh \frac{1}{2}\beta d} \right\} \qquad \text{(III-1)}$$

where $\beta = \left\{ \frac{2G_m}{E_f r^2 \ln(\frac{L}{r})} \right\}^{\frac{1}{2}}$ (III-2)

2L is the interfiber spacing

r is the radius of the fiber

d is the length of the fiber

and the shear stress at the interface is give by:

$$\tau = E_f \epsilon_m \left\{ \frac{G_m}{2E_f \ln(\frac{L}{r})} \right\}^{\frac{1}{2}} \frac{\sinh \beta(\frac{1}{2}d-x)}{\cosh \frac{1}{2}\beta d} \qquad \text{(III-3)}$$

The ratio of maximum interface shear stress at the fiber ends to maximum tensile stress in the fiber can be calculated by equations (II-1) - (II-3), and is found to be:

$$\frac{\tau_{max}}{(\sigma_f)_{max}} = \left\{ \frac{G_m}{2E_f \ln(\frac{R}{r})} \right\}^{\frac{1}{2}} \coth \frac{1}{2}\beta d \qquad \text{(III-4)}$$

If the maximum shear stress that an interface can withstand can be estimated, either experimentally or analytically, then we can calculate the tensile stress in the fiber bundle using equation (III-4). Knowing this critical stress value, σ^* we can then tailor our heating schedule so that the stress in the radial fiber will never exceed this critical value, thereby minimizing micro-cracks that are caused by adhesive failure due to displacement mismatch during the heating up process.

It should be noted that the analysis used here is not exact. Finite element analysis and experimental studies suggested that it underestimates the shear stress concentration at the ends of the fiber by about a factor two. One should always adjust the results from equation (III-3) by a factor of at least two for application, [6].

IV. Heating Rate - Strain Mismatch Approach

During the manufacturing of the billet, the material is subjected to a series of heating and cooling cycles. The significance of shrinkage cracks caused by the contraction of matrix material during cooling is undeniable. Many people have overlooked the possibility that micro-cracks can be generated by displacement mismatch between the fiber and matrix during heating up for reasons that has been discussed in previous sections.

Recall it has been mentioned in section II that the mechanical strain mismatch can be expressed in terms of thermal expansion coefficient mismatch;

$$d\epsilon = (\alpha_m - \alpha_f)\, dT \tag{IV-1}$$

Then the strain rate is

$$\frac{d\epsilon}{dt} = (\alpha_m - \alpha_f)\frac{dT}{dt} \tag{IV-2}$$

The assumption has been made that the billet was subjected to a rapid heating process, so that no significant creep can take place during the heat up. The tensile stress in the yarn at this point will therefore independent of time. By the same token the balancing compressive stress in the matrix must also be time independent. An excessively quick heating rate is undesirable, since it would lead to adhesive failure at the fiber matrix interface. A controlled heating

rate must be used in order to allow creep to partially balance out the strain caused by the mismatch. Assuming creep only take place in the yarn, the strain mismatch which is to be relieved by the creep of the fiber can be equated to the general creep equation;

$$\frac{d\epsilon}{dt} = A(\sigma^*)^n \exp\left[\frac{-\Delta H}{RT}\right] \qquad \text{(IV-3)}$$

σ^* = is the critical tensile stress in which a fiber can withstand without debonding to occur

A = material constant

n = stress exponent

ΔH = activation energy

R = gas constant

T = temperature

If α, E, ΔH, A and n are all temperature independent,

$$\frac{dT}{dt} = \frac{A(\sigma^*)^n}{(\alpha_m - \alpha_f)} \exp\left[\frac{-\Delta H}{RT}\right] \qquad \text{(IV-4)}$$

$$t = \frac{\alpha_m - \alpha_f}{A(\sigma^*)^n} \int_{T_1}^{T} \exp\left[\frac{\Delta H}{RT}\right] dT \qquad \text{(IV-5)}$$

If all the parameters are known, then the rate of temperature change can be found with the tensile stress in the fiber holding at a desirable constant value. The integral of equation (IV-5) will have to be evaluated numerically. The resulting plots will take the shape shown

schematically in Fig.11a, with the stress vs. time curve holding constant as shown in Fig.11b.

V. Heating Rate - Stress Relaxation Approach

When a billet is heated to a elevated temperature, one would expect the highly stressed radial fiber will try to stretch more along the radial direction than the hoop fiber would allow. If a strong bond exists between the radial and circumferential fiber, this will be analogous to the classic model of stress relaxation where the stress in a heated fixed ends rod is being relaxed due to creep.

Assume that the only meaningful creep action is performed by the radial yarn. Recall the unit cell of Fig.9, where the assumption was made that 25% of the cell is radial fiber and the remaining 75% has properties similar to matrix along the radial direction. If balance of force exit between the matrix and fiber.

$$A_m^* \sigma_m = A_f \sigma_f \tag{V-1}$$

where A_m^* = effective area of matrix.

$$0.75\ \sigma_m = 0.25\ \sigma_f \tag{V-2}$$

$$\sigma_m = \frac{1}{3}\sigma_f \tag{V-3}$$

Since the stress term in the creep equation behaves in a power law fashion, this makes the matrix in the radial direction relatively insensitive to creep.

For the creep of the radial fiber, use the general creep equation:

$$\frac{d\epsilon}{dt} = A\sigma^n \exp \frac{-\Delta H}{RT} \qquad (V-4)$$

where ϵ = creep strain.

Since the creep curve of carbon fibers are linear, therefore it is appropriate to apply the steady creep approximation - elastic analogy.

$$\frac{1}{E}\frac{d\sigma}{dt} - A\sigma^n \exp \frac{-\Delta H}{RT} = 0 \qquad (V-5)$$

integrating both sides gives

$$\frac{\sigma^{1-n}}{1-n} = AEt \exp \frac{-\Delta H}{RT} + c \qquad (V-6)$$

Use the initial condition to evaluate the integration constant

At $t=0$, $\sigma = \sigma_e$

where σ_e = stress cause by elastic strain during rapid heat up, before any significant creep has taken place.

c is found to be

$$c = \frac{\sigma_e^{1-n}}{1-n} \qquad (V-7)$$

Substituting back into eqn (V-6)

$$\frac{\sigma^{1-n}}{1-n} = AEt \exp \frac{-\Delta H}{RT} + \frac{\sigma_e^{1-n}}{1-n} \qquad (V-8)$$

$$\sigma^{1-n} = (1-n)AEt \exp \frac{-\Delta H}{RT} + \sigma_e^{1-n} \qquad (V-9)$$

Note that

$$\sigma_e = E\epsilon_e \qquad (V-10)$$

where σ_e = elastic strain

$$\sigma = \left[(1-n)AEt \exp \frac{-\Delta H}{RT} + (E\sigma_e)^{1-n}\right]^{\frac{1}{1-n}} \qquad (V-11)$$

A, n, E, ΔH are to be determined by experiment. For carbon fibers, n has a value greater than one. Equation (V-11) describe the stress in a fiber at any time t for a given temperature T.

The purpose of regulating the stress in the radial fiber is to avoid having the stress exceed a critical stress value σ^*. The temperature versus time and the corresponding stress versus time plot will have shape such as those shown in Fig.12. This heating schedule may be more practical in actual manufacturing practice; unlike the previous method in which the temperature controller has to follow the exact path described by equation (IV-5), this approach allows an approximation to that path.

The stress during the rapid heat up (eq. a-b of Fig.12b) can be calculated quite easily, because the assumption has been made that during the heating process no creep will occur. Therefore stress is caused by both elastic and thermal strain. When the stress value reaches point b, the critical stress value, temperature should hold constant (such as b'-c'at Fig.12a) so that stress can be relaxed (points b-c in Fig.12b) before further heating. The holding time has to be decided by the user depends on the type of fiber. The holding time should not be too long for obvious economic reasons.

VI. The Creep Behavior of an Impregnated Graphite Fiber Bundle

The objective of this study is to determine the stress dependence n and the activation energy $\triangle H$ terms of the well known empirical creep equation,

$$\frac{d\epsilon}{dt} = A\sigma^n \exp\frac{-\triangle H}{RT} \qquad (VI-1)$$

of an impregnated graphite fiber bundle.

The graphite fiber used in this study is Magnamite graphite fiber type HM-3000 which is a continuous high modulus, PAN-based fiber with 3000 filament-count tows. The impregnant used is the CP277-15V coal tar pitch manufactured by the Allied Chemical Corporation.

VI-A Specimen Preparation

Before the specimen can be tested in the high temperature creep furnace, a series of task will have to go into preparing the specimens. A half inch diameter loop was formed at both ends of the dry yarn bundle and was secured with twelve knobs distributed over a two inch section, Fig.13. Cotton sewing tread was used for making the knobs, they should be strong enough to prevent any slipping while being pulled at both ends. The dry yarn measures 16 inches from end to end and is now ready for impregnation.

The 15V coal tar pitch was pretreated at 300C under a nitrogen atmosphere for about five hours before it was used in the actual impregnation of the fiber. The reason for this pretreat process was to drive out some of the undesirable chemicals such as sulfur, ash and hydrogen which made up the pitch. A typical coal tar pitch has a carbon content of 93%, a hydrogen content of 5.5%, a sulfur content of 1.45% and an ash content of 0.05%. These chemicals are highly volatile at high temperature therefore, using untreated pitch as impregnant can cause problems such as the building up of sulfur and ash particles causing the blockage of the nitrogen gas exit tubing and the bloating of the impregnated yarn during the later calcination process.

The graphite fiber bundles were impregnated in pairs,they were laid into a 18 x .75 x .5 inch trench cut out from a rectangular cross-sectioned aluminum. A highly sanded wooden stick was placed at each ends through the hoops of the fiber bundles Fig.14. The function of the sticks was to keep the ends of the fibers above the pitch and for stretching the bundles when it was being raised from the resin bath. The trench was then filled with pretreated 15V pitch powder and was heated on a hot plate. The pitch melts at around 110C and the bundles were allowed to sit in the resin bath for about 2.5 hours to ensure good wetting throughout.

After the fibers were raised from the bath they were put onto a calcination fixture Fig.15. The fixture was made out of fire bricks at both ends with two graphite rods in between. Notice the pivoting mechanism at the left hand side of Fig.15, it was designed to keep the fiber stright at all time during calcination without causing any creep to occur because of the light weight of the material. The entire setup was then put into a tube furnace Fig.16 for calcination.

The instrument used in the calcination process are shown in Fig.17 and 18. Before the furnace was turned on, nitrogen was allowed into the alumina tube at high flow rate to drive air out. Twenty minutes later the furnace was turned on and held at about 30C to allow the heating and sensing elements to stablized. The nitrogen flow rate was then decreased to about two bubbles per second at the water trap and the programmable Honeywell/Brown temperature controller was turned on. Below 300C the heating rate was 100C/hr.; :from 300C to 750C which is the critical temperature range the heating rate was about 15C/hr.; from 750C to 900C the heating rate was about 50C/hr. The heating history of each pair of fiber bundles was recorded on a plotter for later reference. At about 900C the furnace was turned off and allow to cool to room temperature with nitrogen flowing at all time to insure minimal oxidation.

VI-B Creep Experiment: Instrumentations and methodology

The creep experiment was performed at a facility in the Aerospace Corporation's Material Science Laboratory. The instrumentations used are shown in Fig.19 and 20. The calcined fiber bundle was held in place inside the high temperature creep furnace by two mechanisms shown in Fig.21, These clamping mechanisms were machined out from a very fine grained graphite. One end of the fiber was fixed and the other end unrestrained. the unrestrained end was connected to a weight which passed over a smooth pulley. A linear variable digital transducer (LVDT) is also connected to this free end, any yarn displacement would be detected by the LVDT. The signal sent out by the LVDT will then be measured by a digital volt meter (DVM) and recorded in voltage by a HP9815 computer. The computer was so programmed that a reading was taken every three minutes and forty-five seconds. When the computer takes a reading, a glitch maker which was connected to the computer and a two channel chart recorder would make a spike on the chart at that instant which aids in later data interpretations. The furnace current was controlled manually below 1500C and was then switched over to computer monitoring over 1500C. Below 1500C the temperature was measured by a manual optical pyrometer, at above 1500C the temperature was measured by a IRCON Infrared pyrometer which was connected to the same two channel chart recorder. which means that the chart recorder

will not start recording temperature readings until the furnaced reached 1500C. Since significant creep usually take place at temperature above 2200C for this material, no important data is lost from such an arrangement.

The stress dependence of the creep rate was determined by a change-of-stress method in which the structural changes which usually take place during creep is minimized. In this unispecimen method each specimen was strained at a selected temperature under an argon atmosphere and stressed until the creep curve was well established, at which time the stress was changed suddenly to another value while holding the temperature constant. The ratio of the creep strain rate immediately after the stress change to that just before is compared to the ratio of stress after the change to that immediately before to determine the stress dependence of the creep rate. The stress dependence was found to take the following form:

$$n = \frac{\ln \dot{\epsilon}_2/\dot{\epsilon}_1}{\ln \sigma_2/\sigma_1} \qquad \text{(VI-2)}$$

where $\dot{\epsilon}_2$ and $\dot{\epsilon}_1$ are the creep rates immediately after and immediately before the change, and σ_2 and σ_1 are the respective stresses. Since the structure immediately before and after the stress change was essentially the same, the structural differences that normally complicates analyses of the stress dependence of the creep rate does not exists.

The same line of reasoning is applied to determine the activation energy of the impregnated bundle. This time we change the temperature while holding other variables, stress and structure constant. Knowing the temperature difference and the creep rate at respective temperatures, the activation energy is found to be in the following form:

$$\Delta H = \frac{R\, T_1\, T_2}{T_2 - T_1}\left[\ln \epsilon_2 - \ln \epsilon_1\right] \qquad \text{(VI-3)}$$

The scattering of ΔH and n values is expected despite the outmost care that has gone into preparing and testing the specimens. A best fitted value will have to be chosen for each of the two parameters, they are in turn used to determine the material parameter A of the general creep equation (V-4).

expressed as

$$\dot{\epsilon}_{tot} = \frac{1}{N} \sum_{i=0}^{10} \dot{\epsilon}(x_i)$$

where N=11 is the number of divisions. It was found that this total average strain rate differs from the creep rate calculate only from the highest temperature region by less then one percent. This shows that using the six inches uniform hot zone to be the gauge length is a very good approximation.

The activation energy ΔH of the yarn was determined by the unispecimen change of temperature technique which has already been discussed earlier. The results are shown in Fig.24 through 29. The data points in the figures were fitted with a straight line using the method of linear regression. The slopes of these lines are proportional to the activation energy of the impregnated yarns. The numerical results of the activation energy are in surprisingly good agreement. The mean value for ΔH is 61.68 kcal/mole with a standard diviation of only 2.2 kcal/mole.*

The stress dependence n of the yarn were to be determined by the unispecimen change of stress method, but was forced to change the plan when unexpected problems arose. The first disadvantage of the unispecimen change of stress method is the changing of the stress, especially at

*The physical interpretations of the activation energy are presented in Addendum II.

VI-C Creep Experiment: Results

The creep rate of an impregnated HM-3000 fiber was obtained by converting the rate of voltage change recorded by the HP9815 computer into elongation rate in mm/hr. All the temperature data points obtained during a temperature raise were neglected, this is because elongation recorded during this period were resulted mainly from thermal expansion of the fiber. Only those datas points which were recorded after the furnace temperature has stablized were selected. Assumption has been made that all of the creep occurred at the six inches uniform hot zone located at the center portion of the three feet long furnace. Analysis performed by Feldman [7], proved that this is a very good approximation.*

In the analysis the temperature distribution of the furnace was assumed to be hyperbolic Fig.22. Because of symmetry of the distribution only one side of the furnace will have to be analyized. The furnace was then hypothetically divided into ten sections along its length, and the fibers were allowed to creep independently with respect to the average temperature at their own specific location. A creep strain versus location curve can then be plotted, and the results are shown in Fig.23. When the average creep rate at each section are summed numerically, the result is the total average creep strain and can be

* Addendum I presents further discussion of the gage length and the calculation of the pre-exponential factor A of Equation (VI-1).

temperature in the excess of 2300 C. At this temperature any change in load can trigger failure even if it was performed by a very steady hand. Another problem associated with the changing of weight is that when a load is added or taken off from a fiber, the fiber will shift to the right or to the left depends on which action was undertaken. The sudden shift of a fiber will interrupt the delicately focused IRCON infrared pyrometer which controls the furnace current. If a cold spot is exposed to the pyrometer the furnace current will shoot up suddenly and vise versa. It will take a long time for the furnace to stabilized and even more difficult to get it back to the exact temperature as it was before the load change. The most curious phenomenon was that after a fiber was hot stretched at a certain load no creep was detected at that same temperature even when the load was increased by 300%. It was noticed that creeping reassumed when temperature is raised aboved the previous hot stretching temperature, but at a rate much lower than expected as shown in Fig.28 and 29. All these factors made it very difficult to use the unispecimen change of stress method to determine the stress dependence.

An alternate method was to compare the creep rates at the same temperature for two constant load trails. One can argue that the unispecimen method may be is very important for working with materials like highly-oriented polycrystalline graphite, but not necessary so for testing

fibers. Since all the specimens used were made from the same roll of fiber, properties homogeneity is assured. Variations can only came from the impregnation and calcination procedures. Every effort has been made to ensure that the specimens' preparation procedures were as uniform as possible. Random testing has confirmed that the matrix weight fractions were about 65% on various specimens. In the light that we have exactly identical dry fibers, reasonably uniform impregnation/calcination procedures and also the fact that nearly most of the load were carried by the fiber, one can conclude that this method is valid.

The calculated values for the stress dependence are listed on table(3), and found to be varied from 1.2 to 2.1. After careful eliminations of bad data, a mean n value of 1.41 with a standard deviation of .13 was found. This suggested that an impregnated HM 3000 fiber has some viscous behavior, for which the creep rate is nearly proportional to the applied stress. The stress dependence of viscous creep material is one.

Conclusion

The findings of the crack study performed by Kuhansedgh and Sines [1] hinted that the level of stress in the fiber bundle may have something to do with the crack pattern observed. The assumption that the radial fiber is the most severely stressed fiber is confirmed by a simple analysis. The usefulness of a strong and well bonded radial fiber in reducing processing anomalies was reviewed by modifying the computer model developed in [1]. Note that the billet will benefit from the radial fiber only if the radial fiber is strong and well bonded. If the radial fiber debonds during processing, its effectiveness in relieving hoop stress is minimal and would be economically unfounded to weave in the radial yarns to begin with. In the light of this problem two different methods were devised, namely, the fiber/matrix displacement mismatch approach and the stress relaxation approach. The aim of these two methods were to develop a heating schedule which takes advantage of the creep action of the fiber as a stress relieving agent, to keep the radial fiber from debonding thereby preserving its intended usefulness to the billet.* Two important parameters of the general creep equation, the activation energy and stress dependence for an impregnated HM 3000 fiber bundle were determined by experiment, they took up a value of 61.68 kcal/mole and 1.41 respectively.

---

* Further analysis and discussion of the optimum time-temperature path are presented in Addendum III.

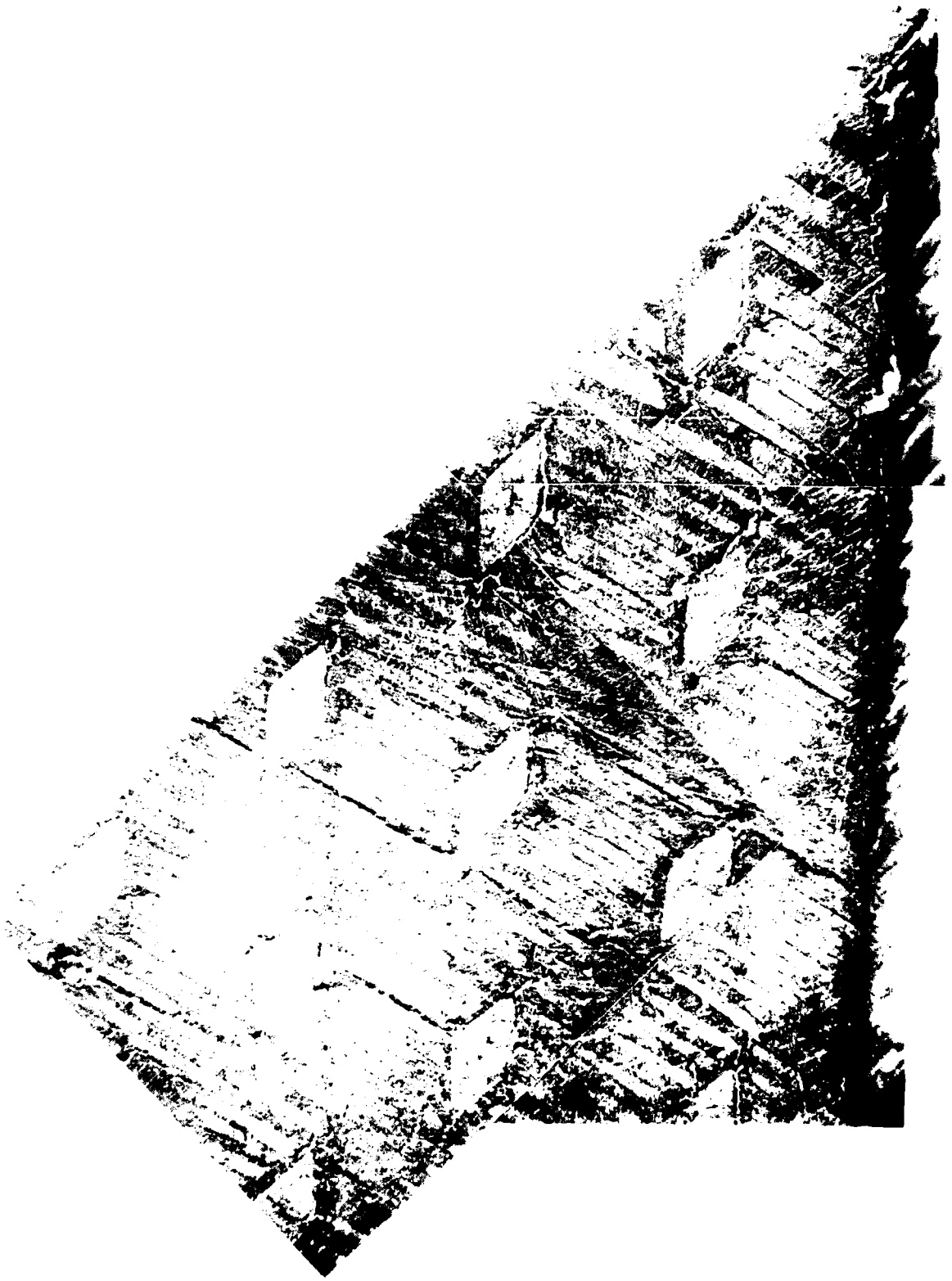

Fig.1 Picture showing a (111) plane cut from the [illegible] fillet

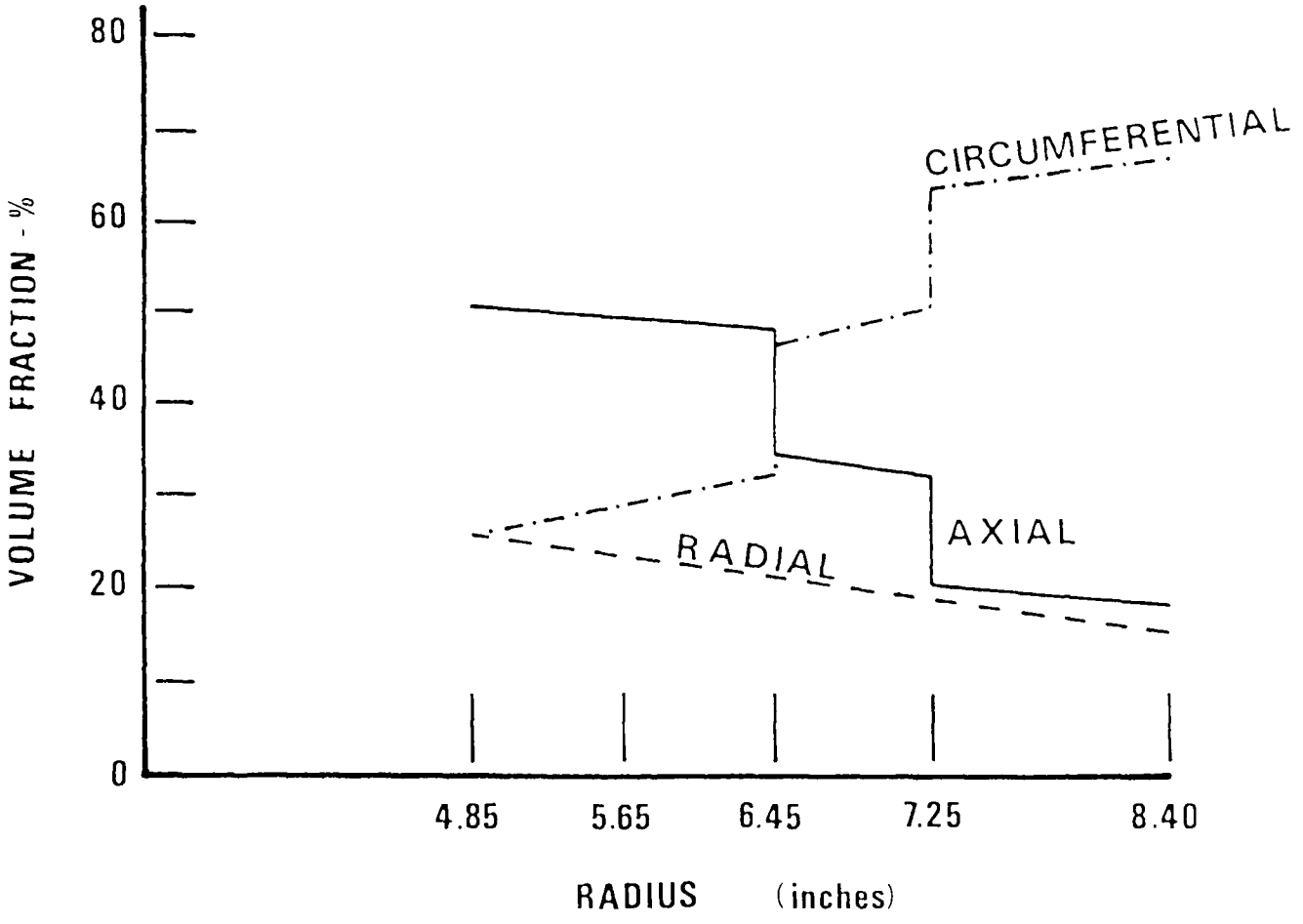

Fig. Variation of Fiber Volume Fraction with Radius of the Billet

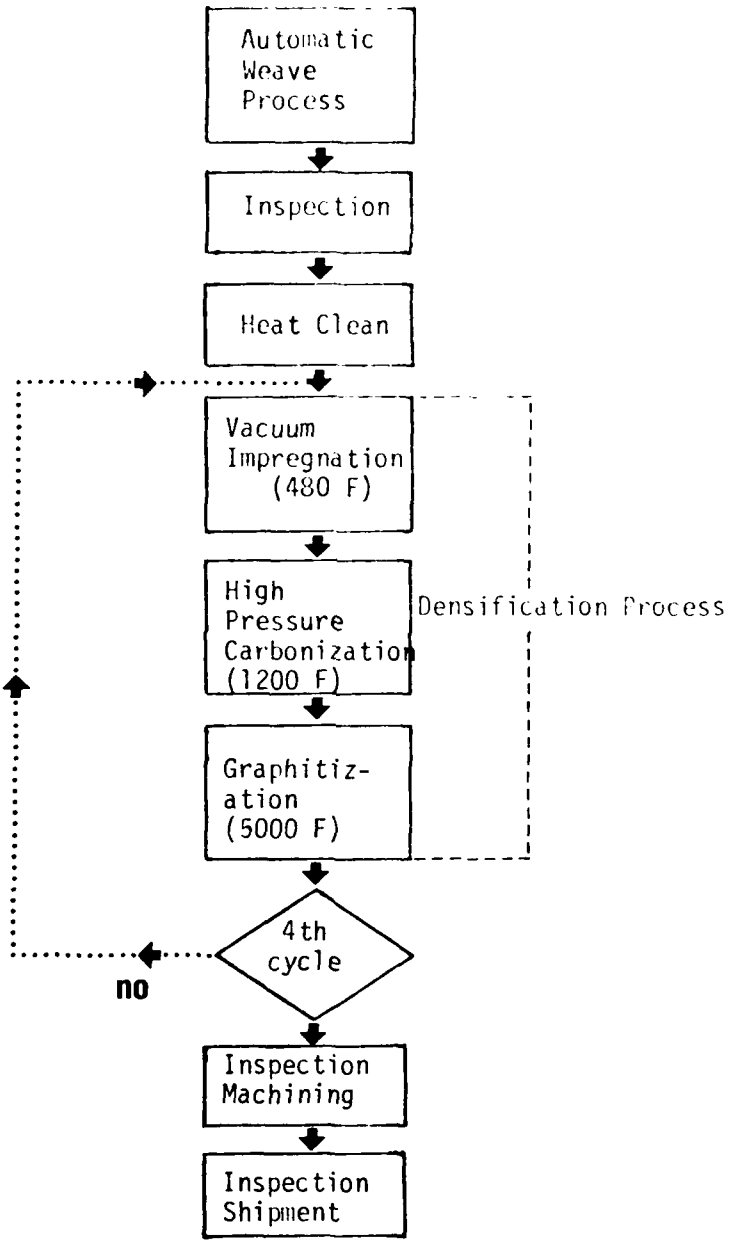

Fig.3 Process Flow Chart of the Billet

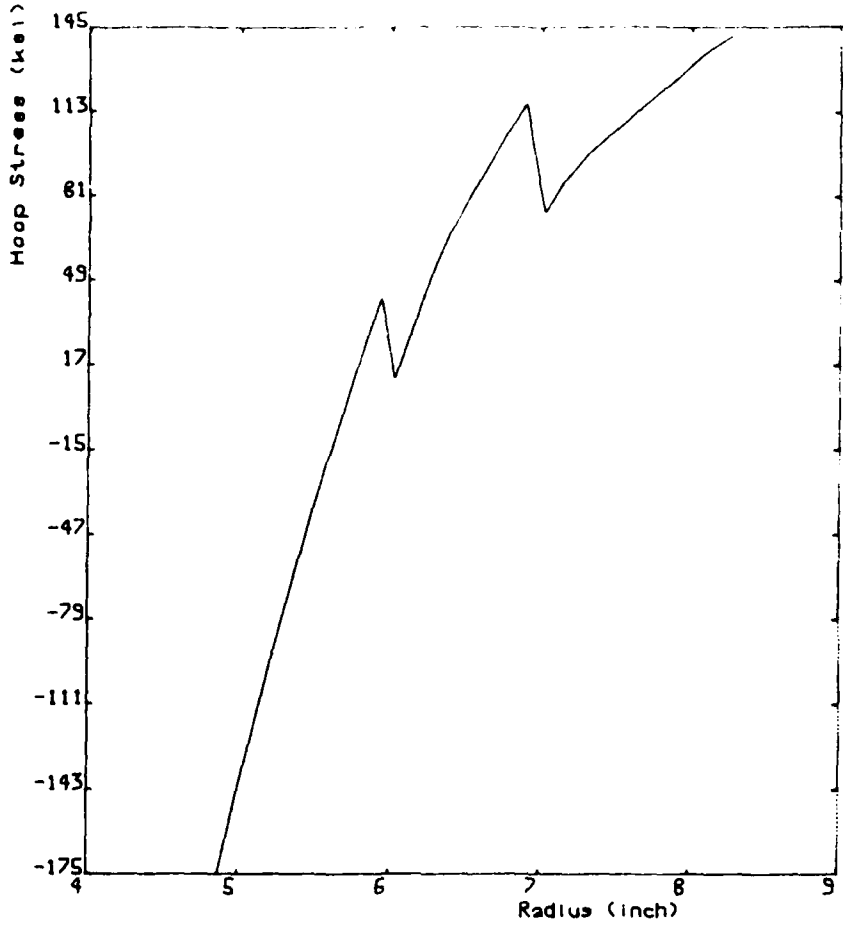

Fig.4 Hoop Stress vs Billet Radius Without the Radial Effect

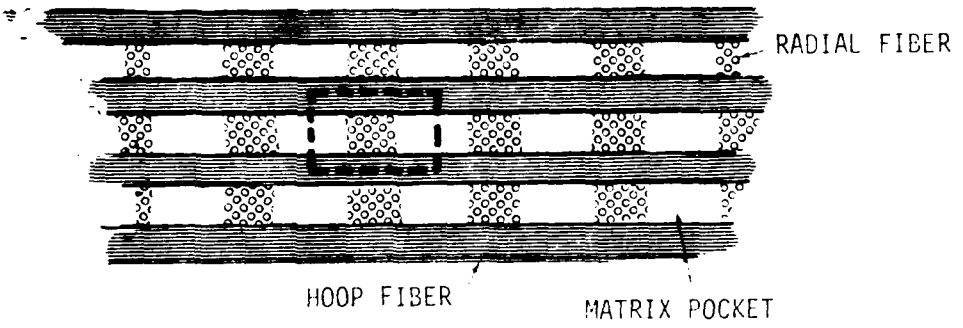

Fig.5 Diagram Showing A Characteristic Area on the Billet's Cylindrical Surface

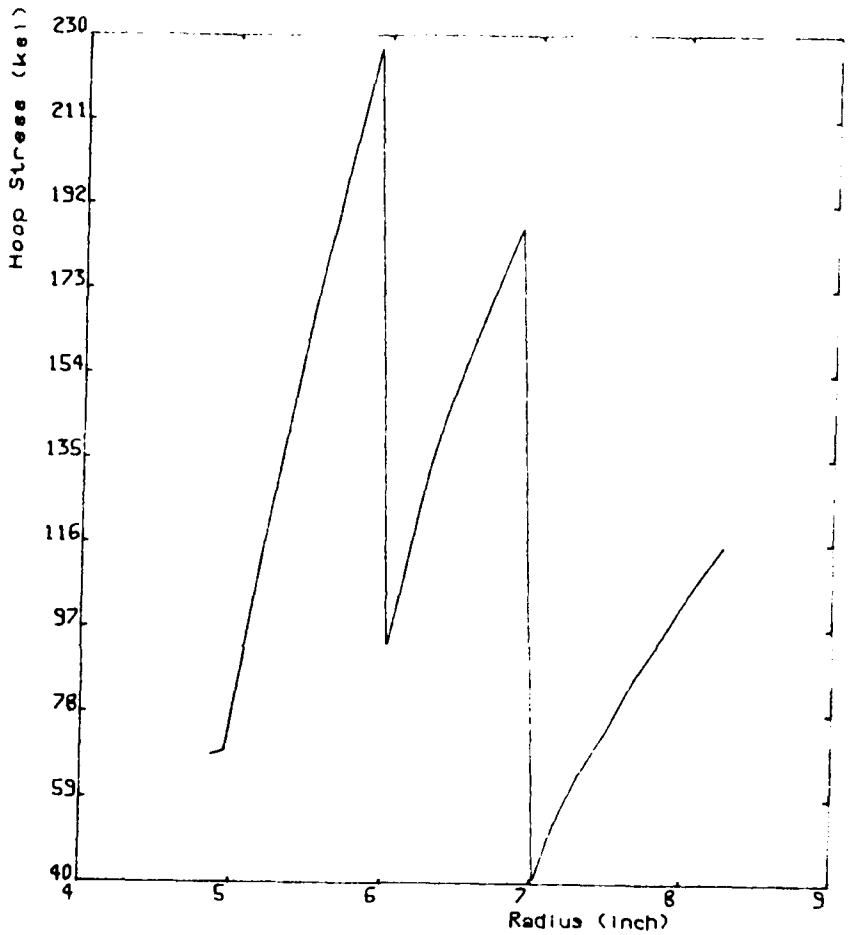

Fig.6 Hoop Stress vs Billet's Radius With the Radial Effect

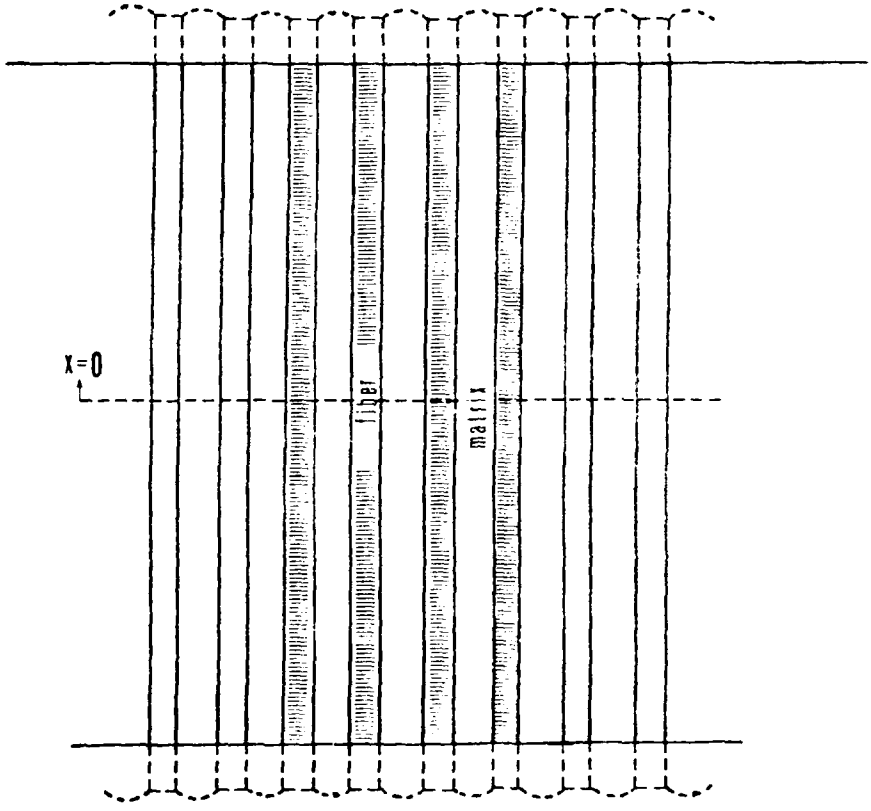

Fig.7 Billet With Equally Spaced Fiber and Matrix. (The dotted lines repersents the shape that the billet takes just after a rapid heat up)

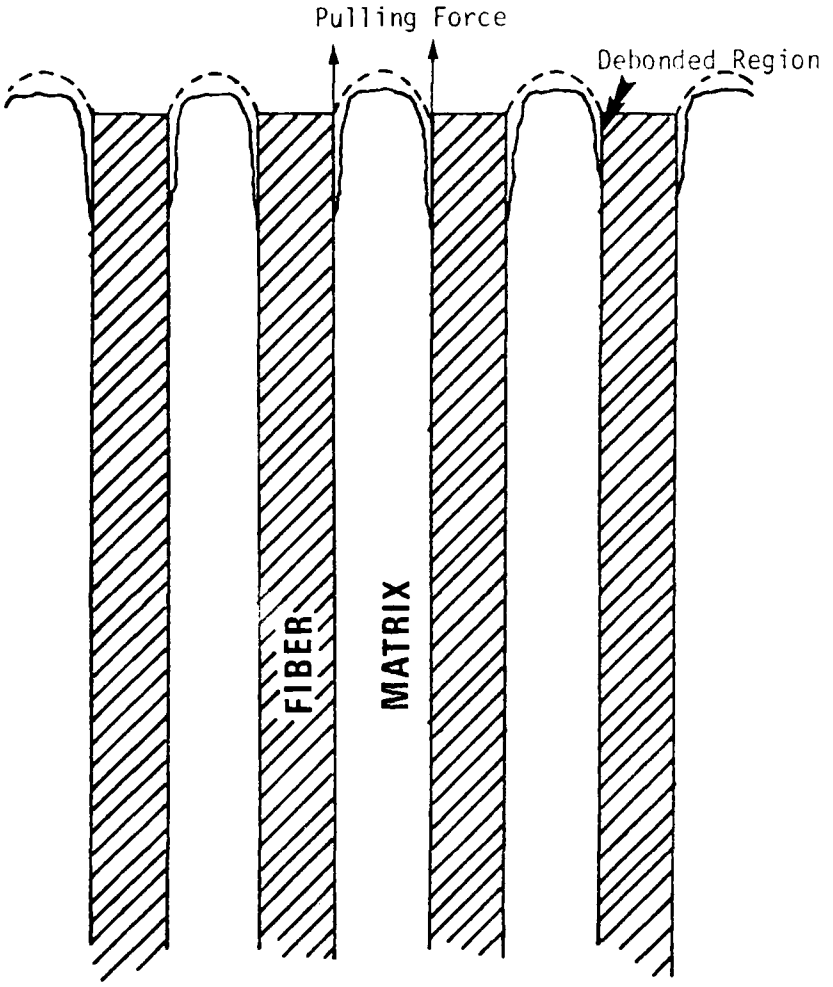

Fig.8 Forces Acting at the Fiber Matrix interface due to Mismatch in Coefficient of expansion, and Modulus

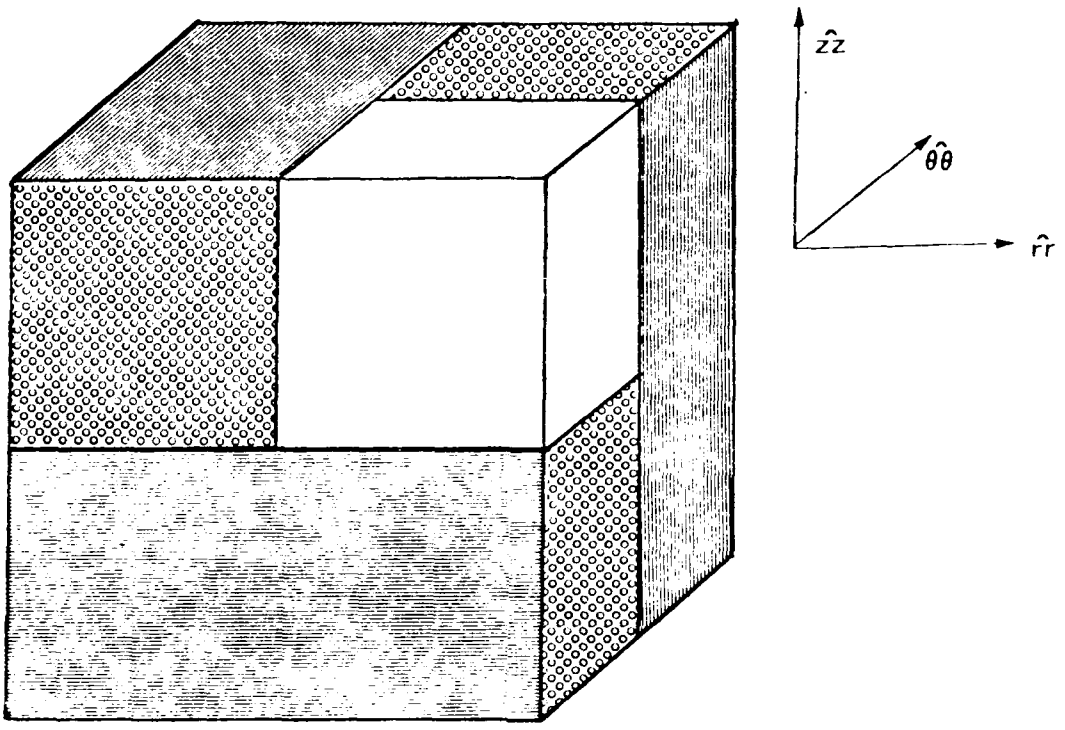

Fig.9 A Characteristic Unit Cell of the Billet

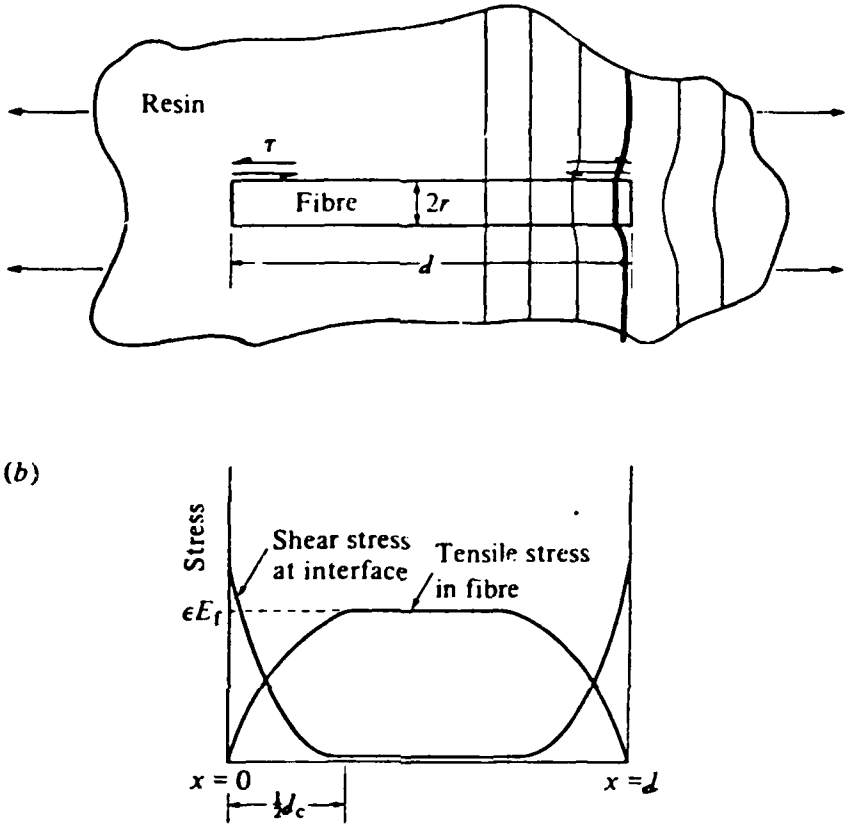

Fig.10 a. Diagrammatic representation of deformation around a discontinuous fiber embeded in a matrix subject to a tensile load parallel to the fiber.

b. Stress distribution at the interface and in the fiber.

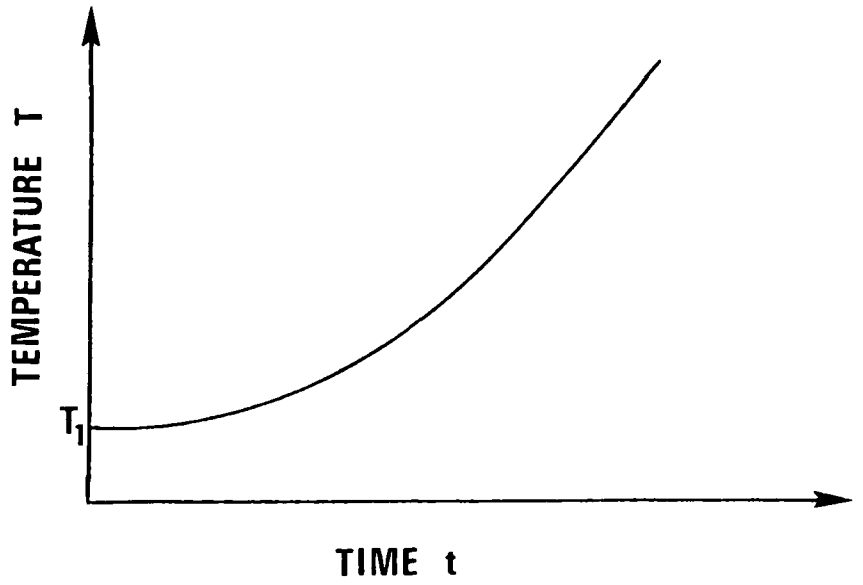

Fig.11a A typical T vs. t plot

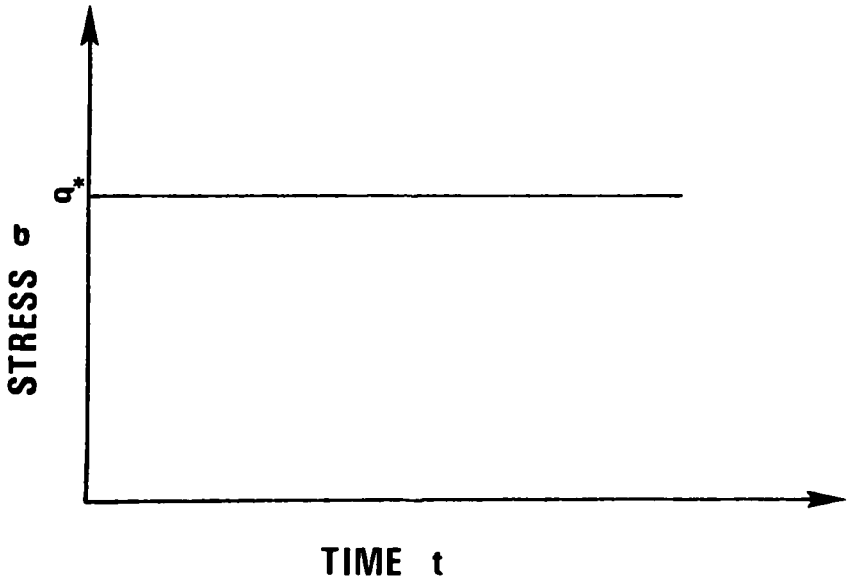

Fig.11b A typical stress vs. t plot

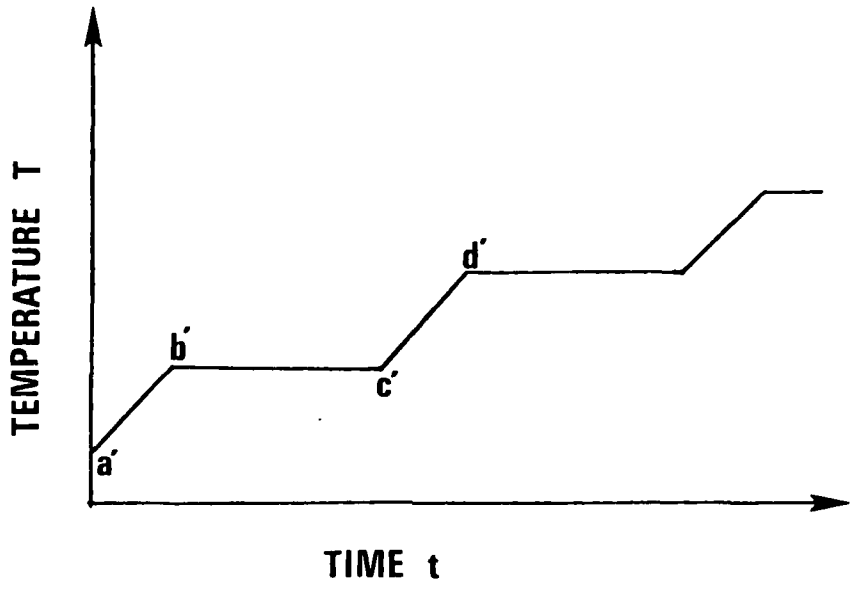

Fig.12a A typical T vs. t plot

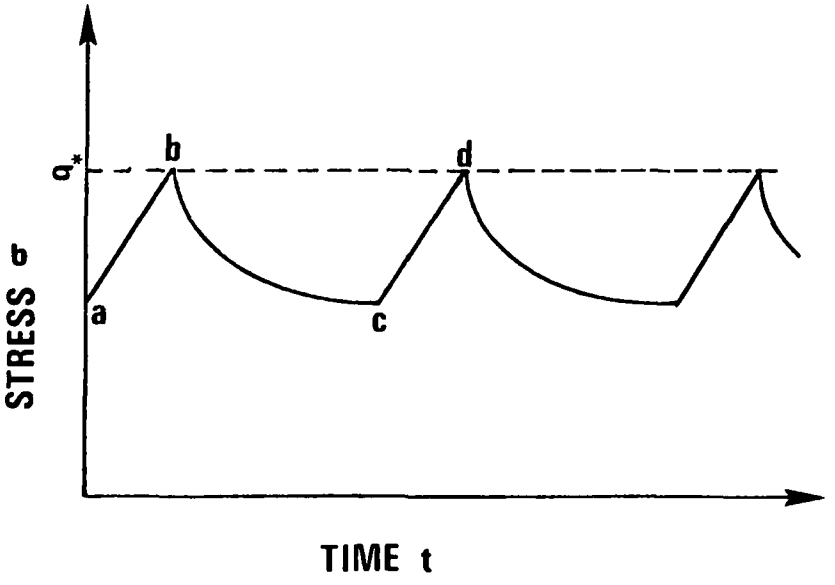

Fig.12b A typical stress vs. t plot

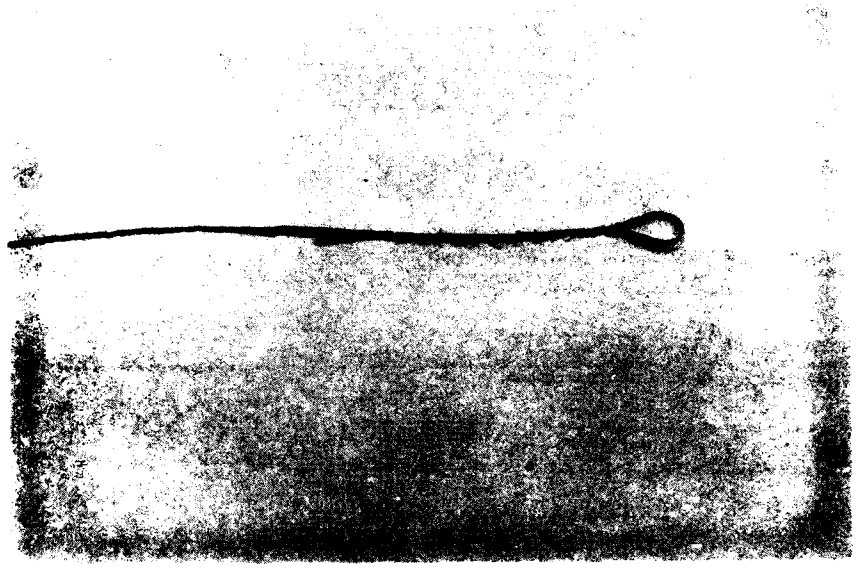

Fig.13 The overlap preparation of the specimen

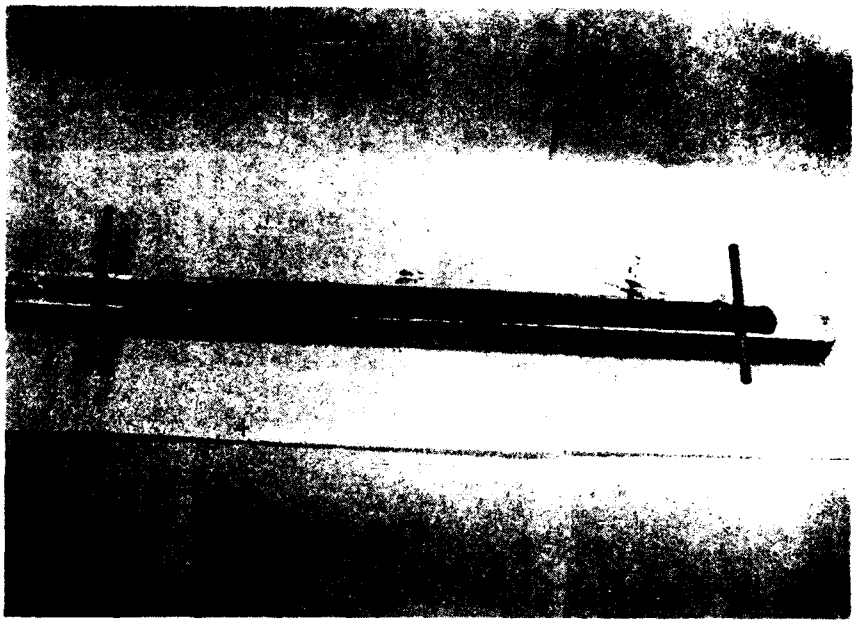

Fig.14 The impregnation fixture

Fig.15 The calcination fixture

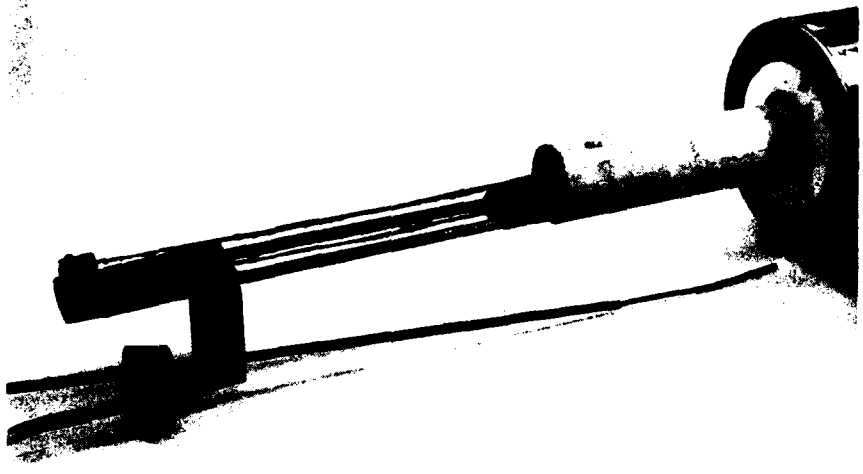

Fig.16 The calcination fixture loaded with specimen ready for the tube furnace

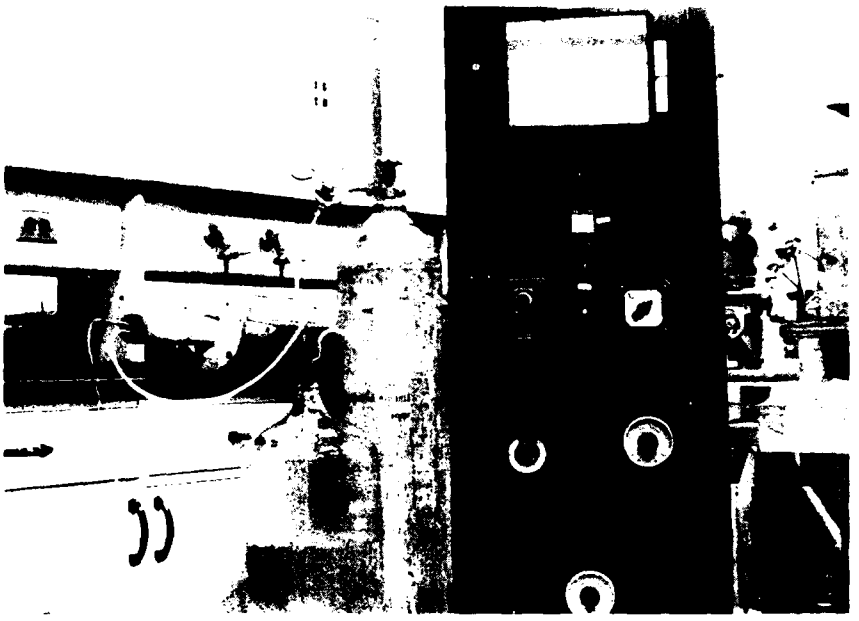

Fig.17 Instrumentation used in the calcination process

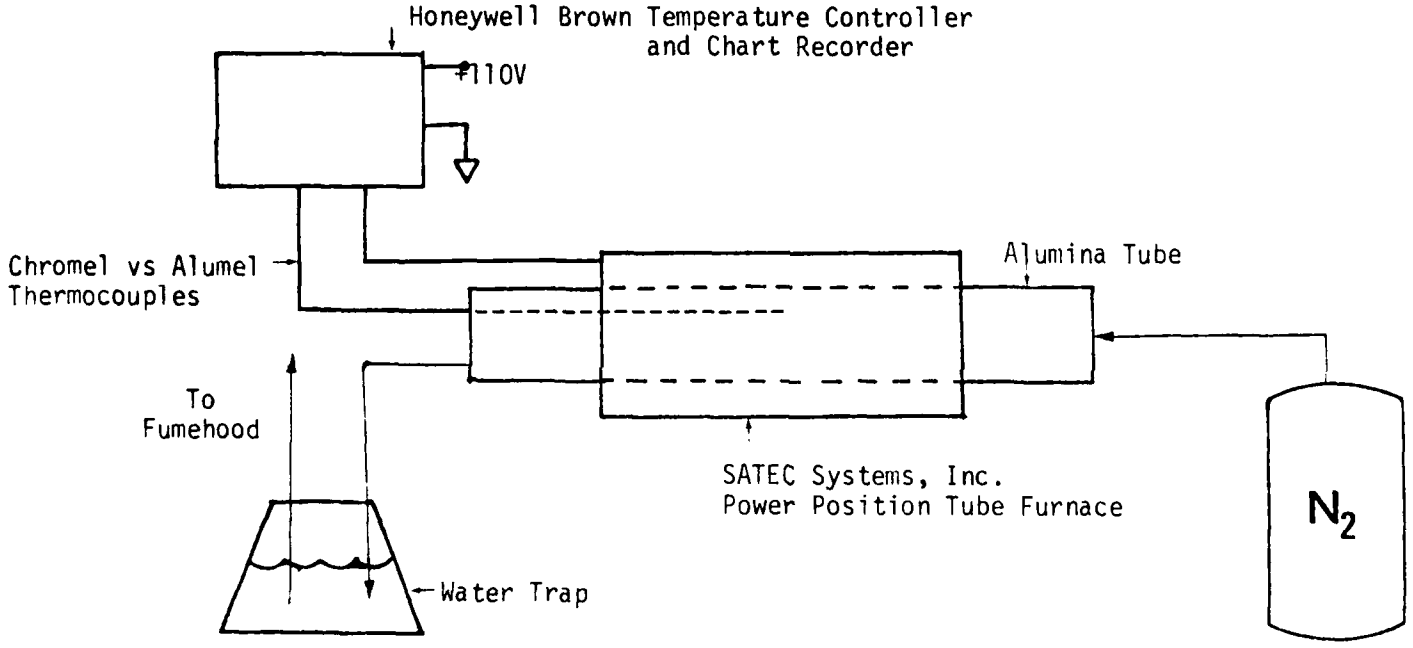

Fig.18 Block diagram of the instruments used in the calcination process

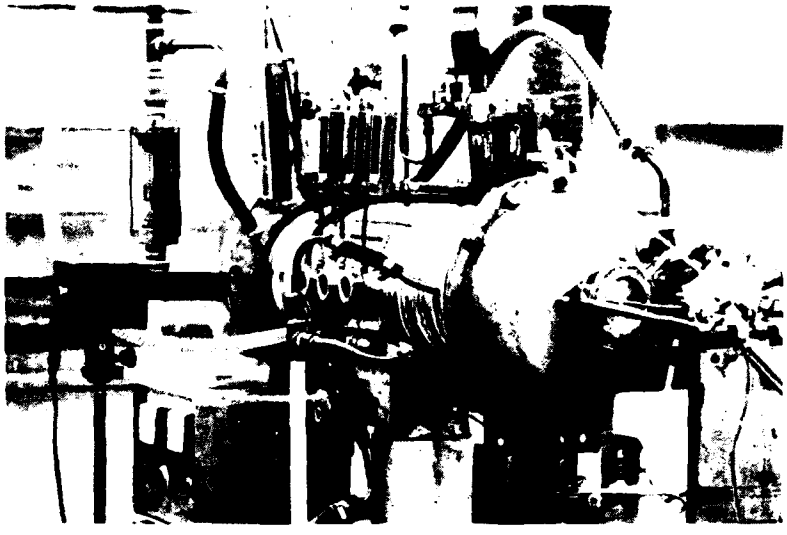

Fig.19 High temperature furnace used in the creep experiment

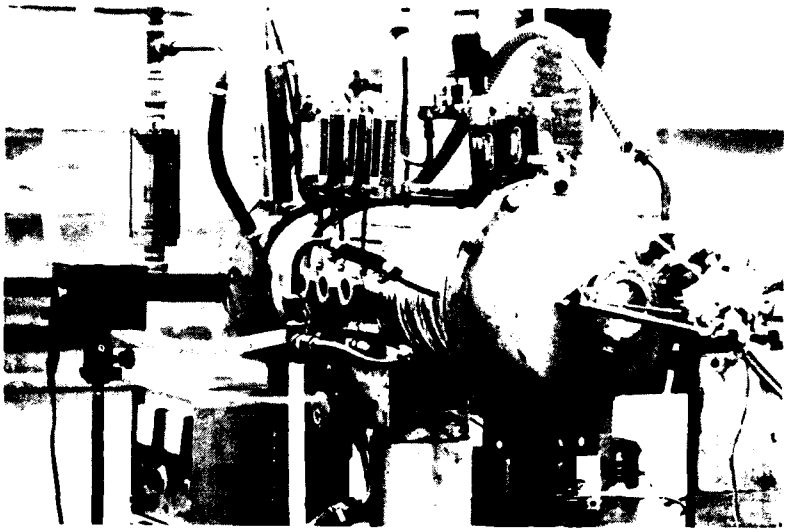

Fig.19 High temperature furnace used in the creep experiment

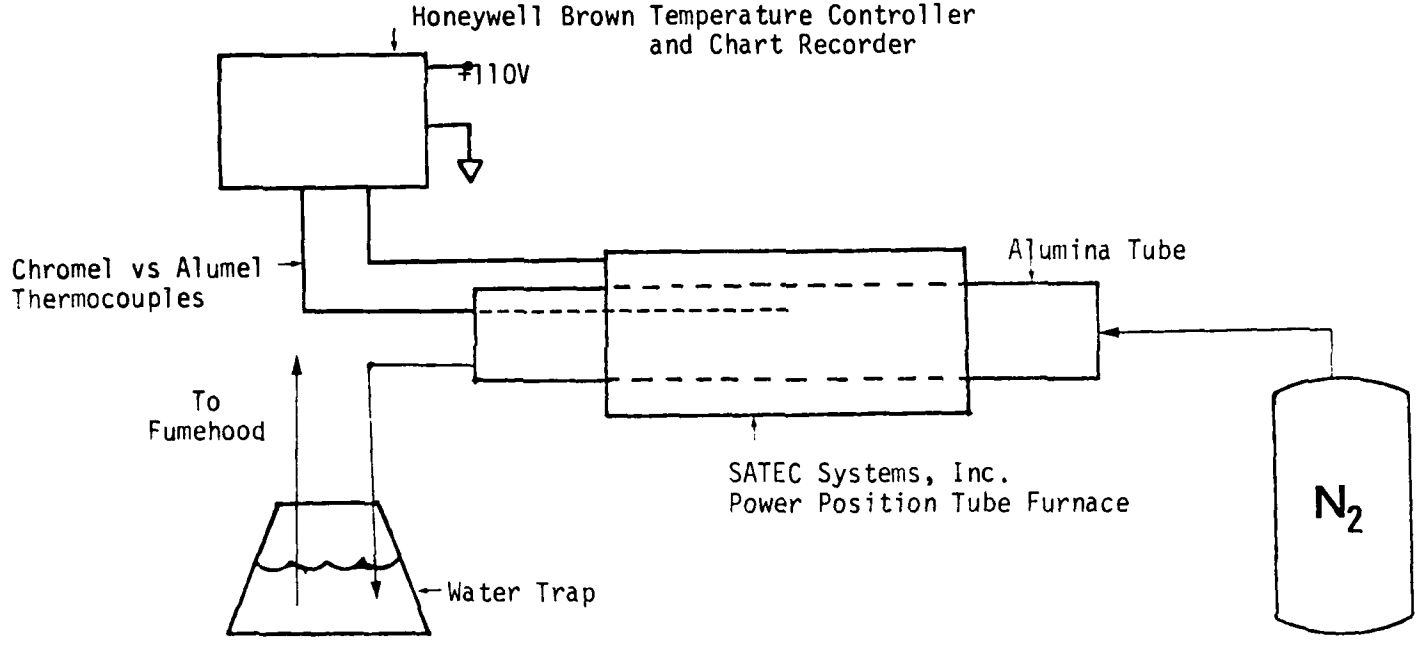

Fig.18 Block diagram of the instruments used in the calcination process

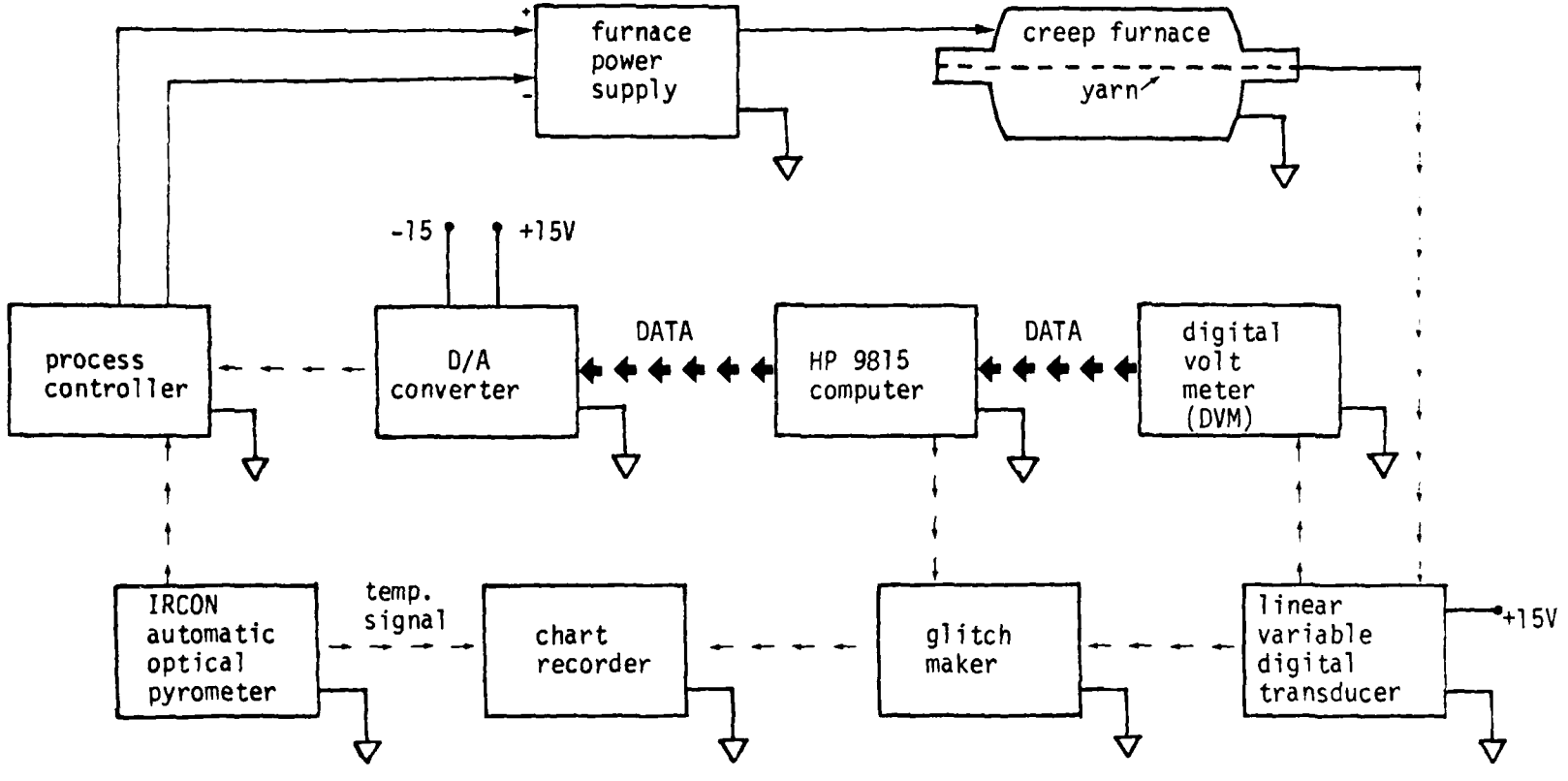

Fig.20 Block diagram of the instruments used in the creep experiment

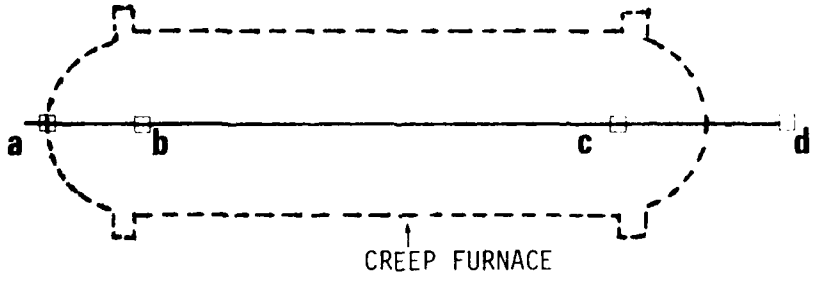

a. FIXED END

b,c. GRAPHITE CONNECTING PINS

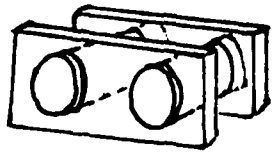

d. GRAPHITE SCREW CONNECTING DIRECTLY TO THE LVDT UNIT

Fig.21 Specimen clamping mechanisms used in the creep experiment

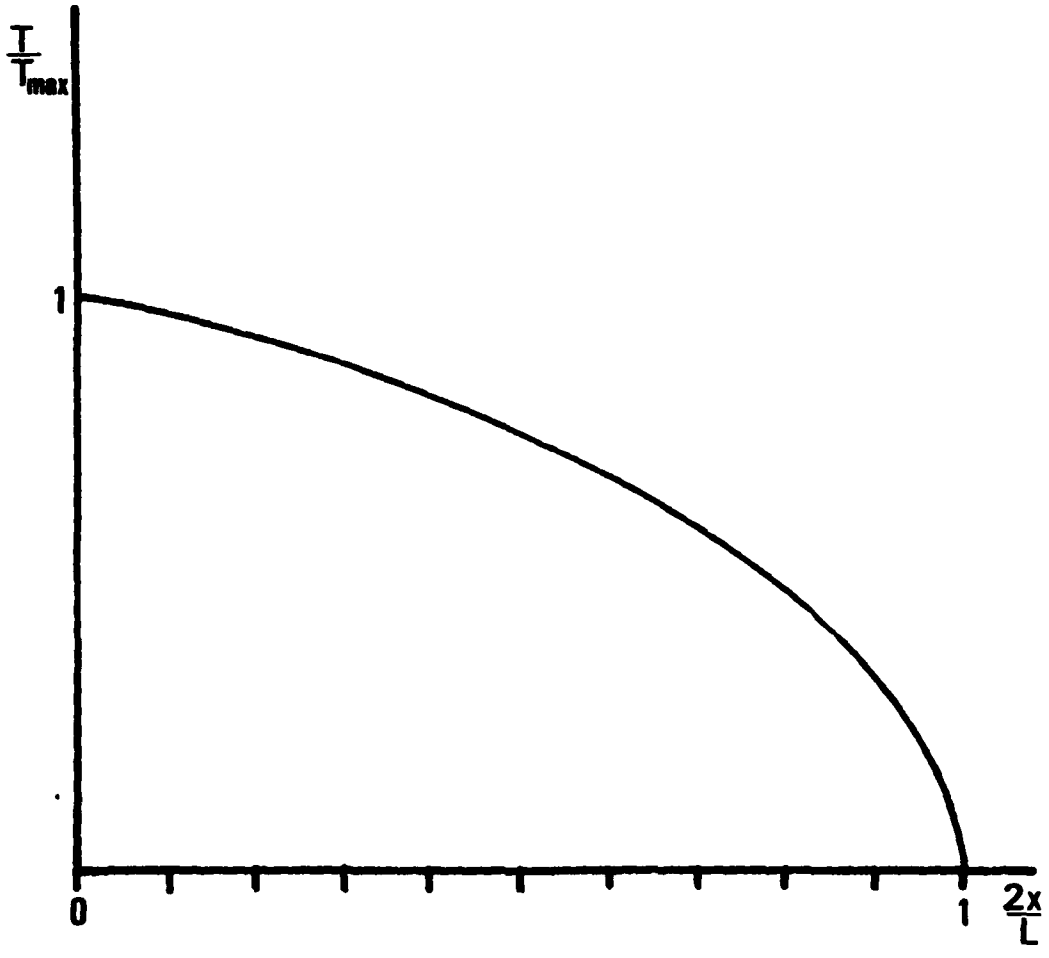

Fig.22 Hyperthetical temperature distribution of the creep furnace

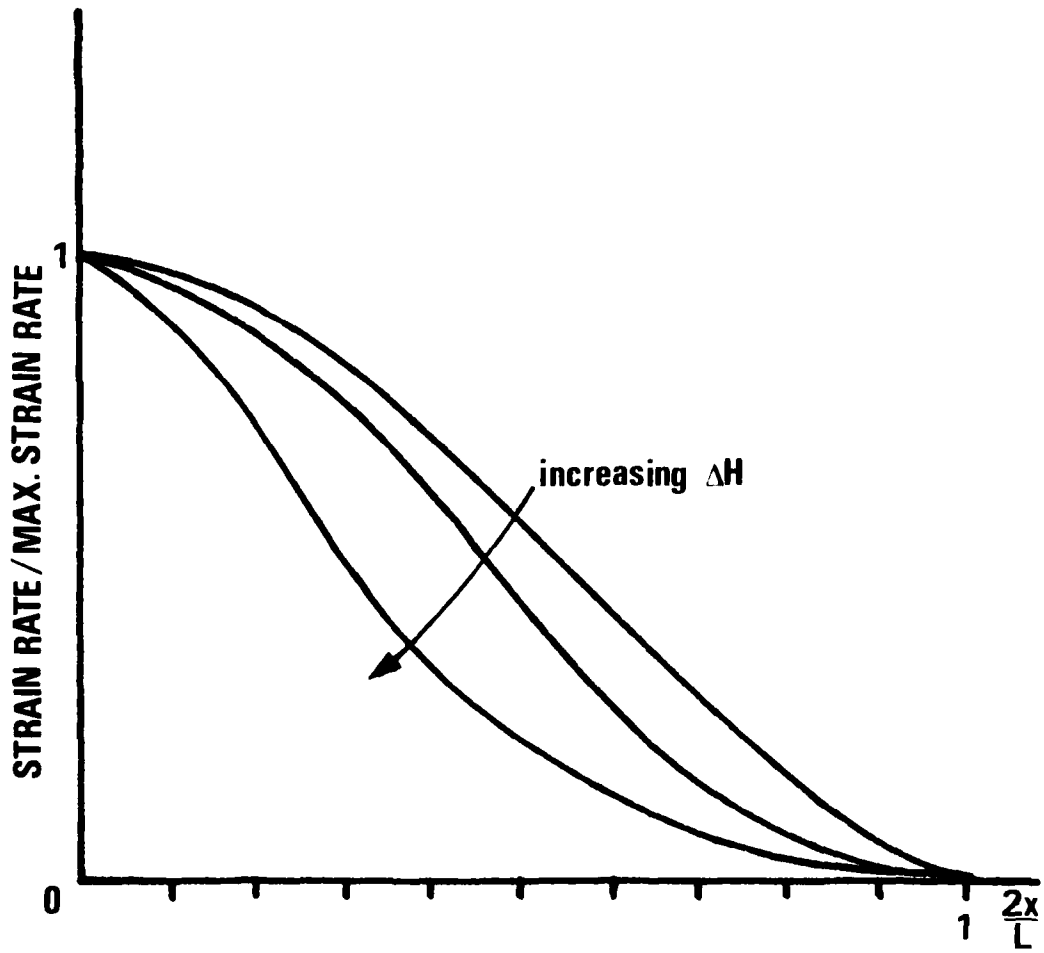

Fig.23 Normalized creep rate vs. location in the creep furnace

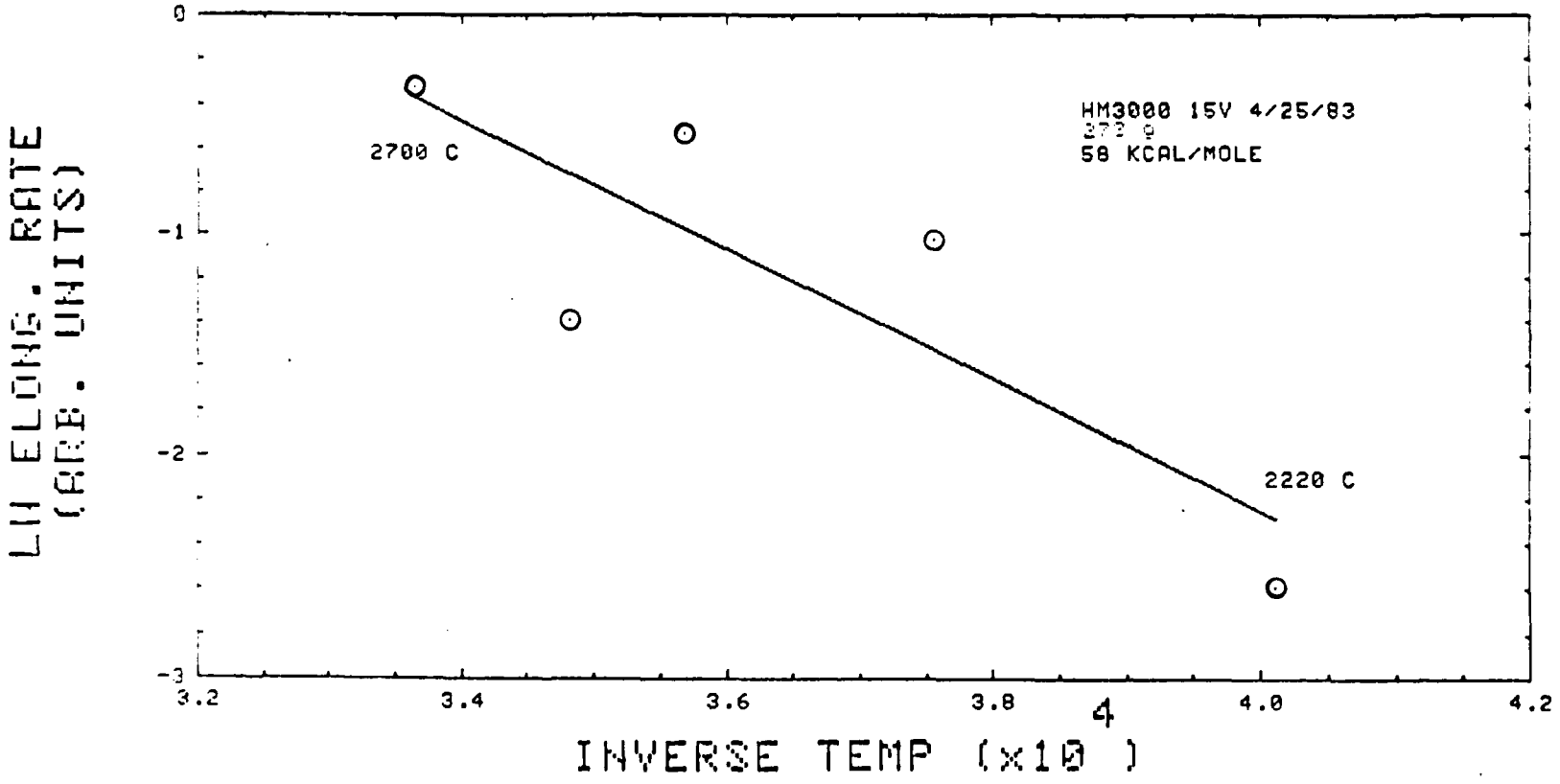

Fig.24 Creep elongation rate vs. inverse of absolute temperature

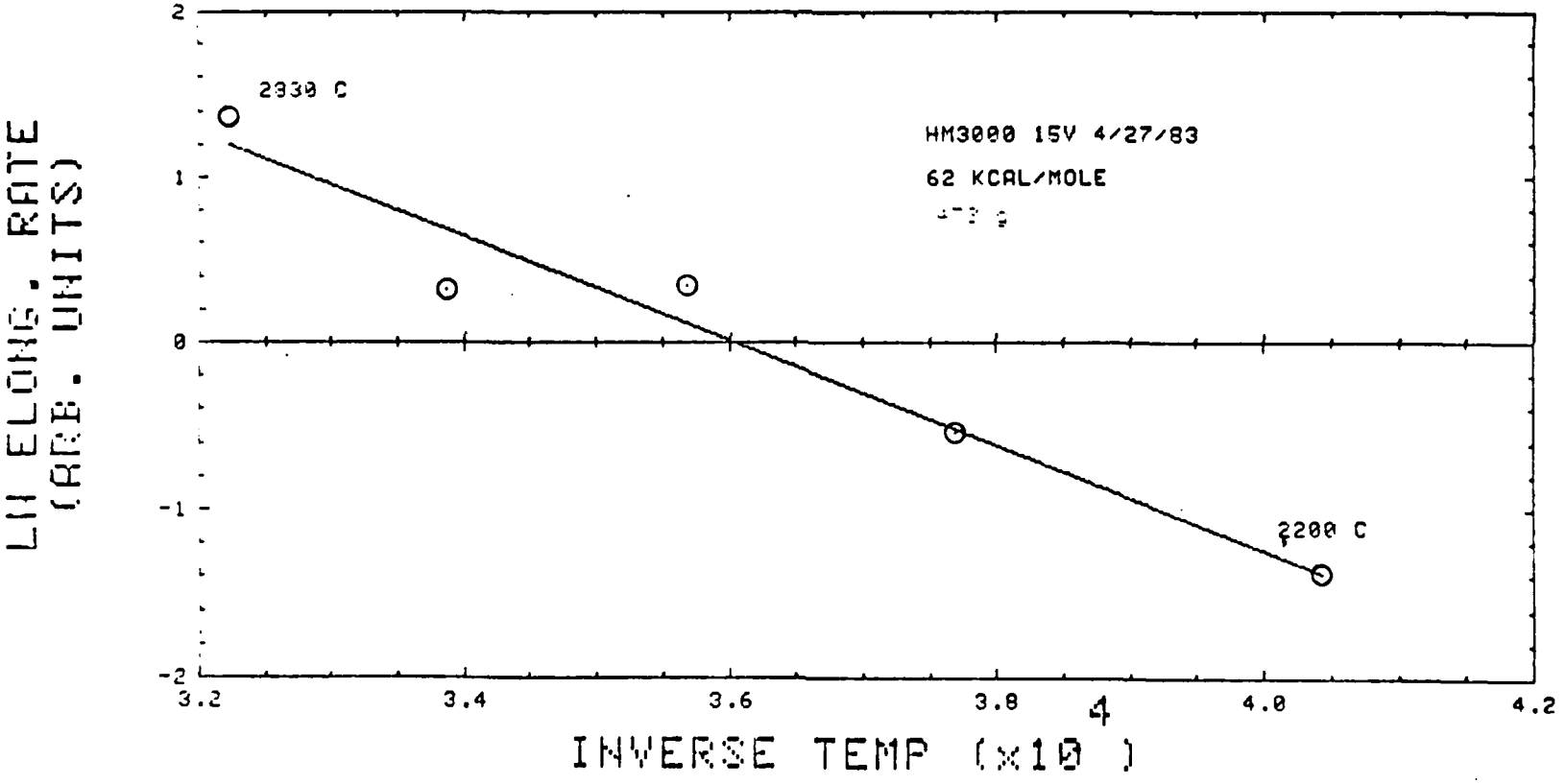

Fig.25 creep elongation rate vs. inverse of absolute temperature

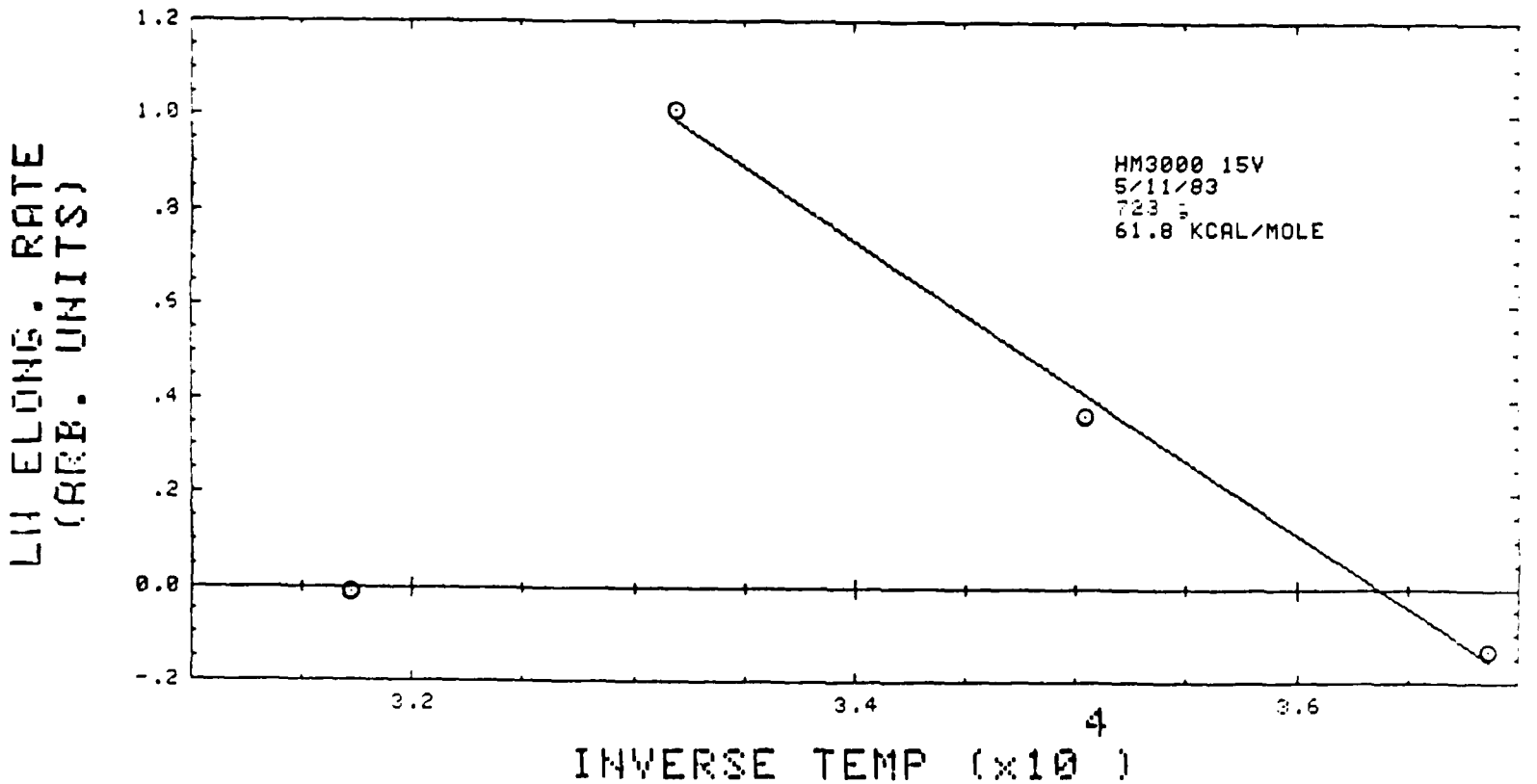

Fig.26 creep elongation rate vs. inverse of absolute temperature

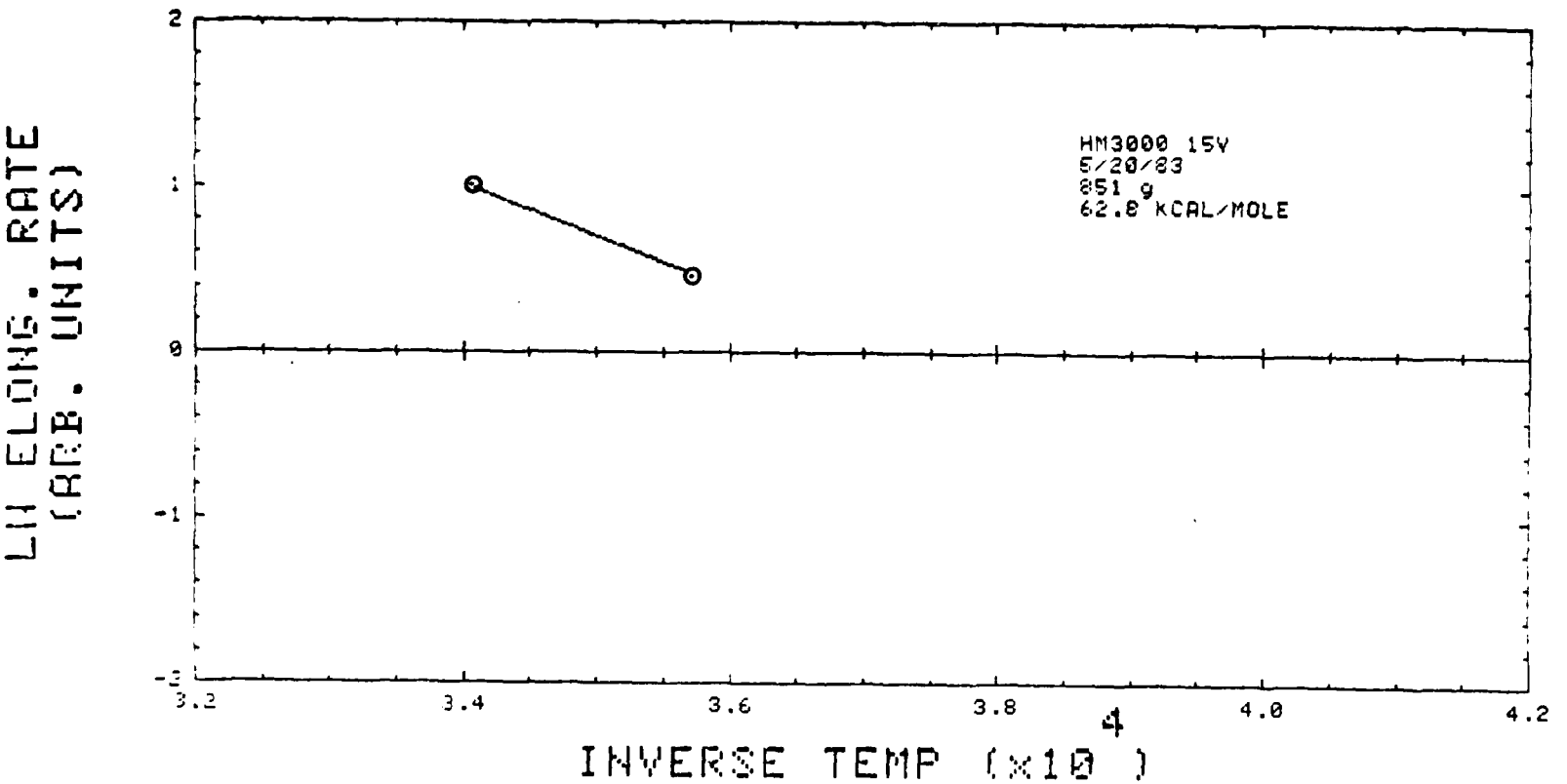

Fig.27 creep elongation rate vs. the inverse of absolute temperature

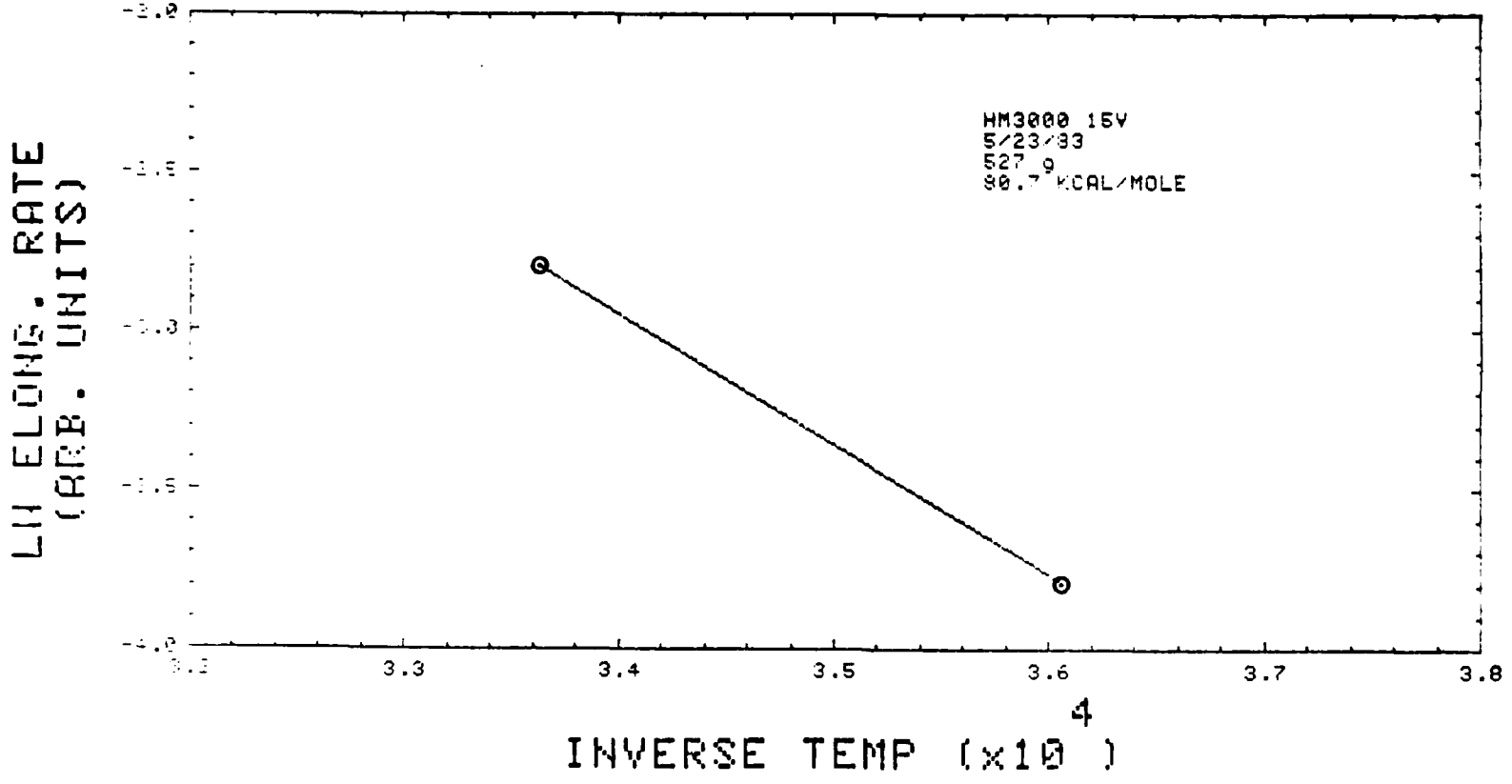

Fig.28 creep elongation rate vs. the inverse of absolute temperature

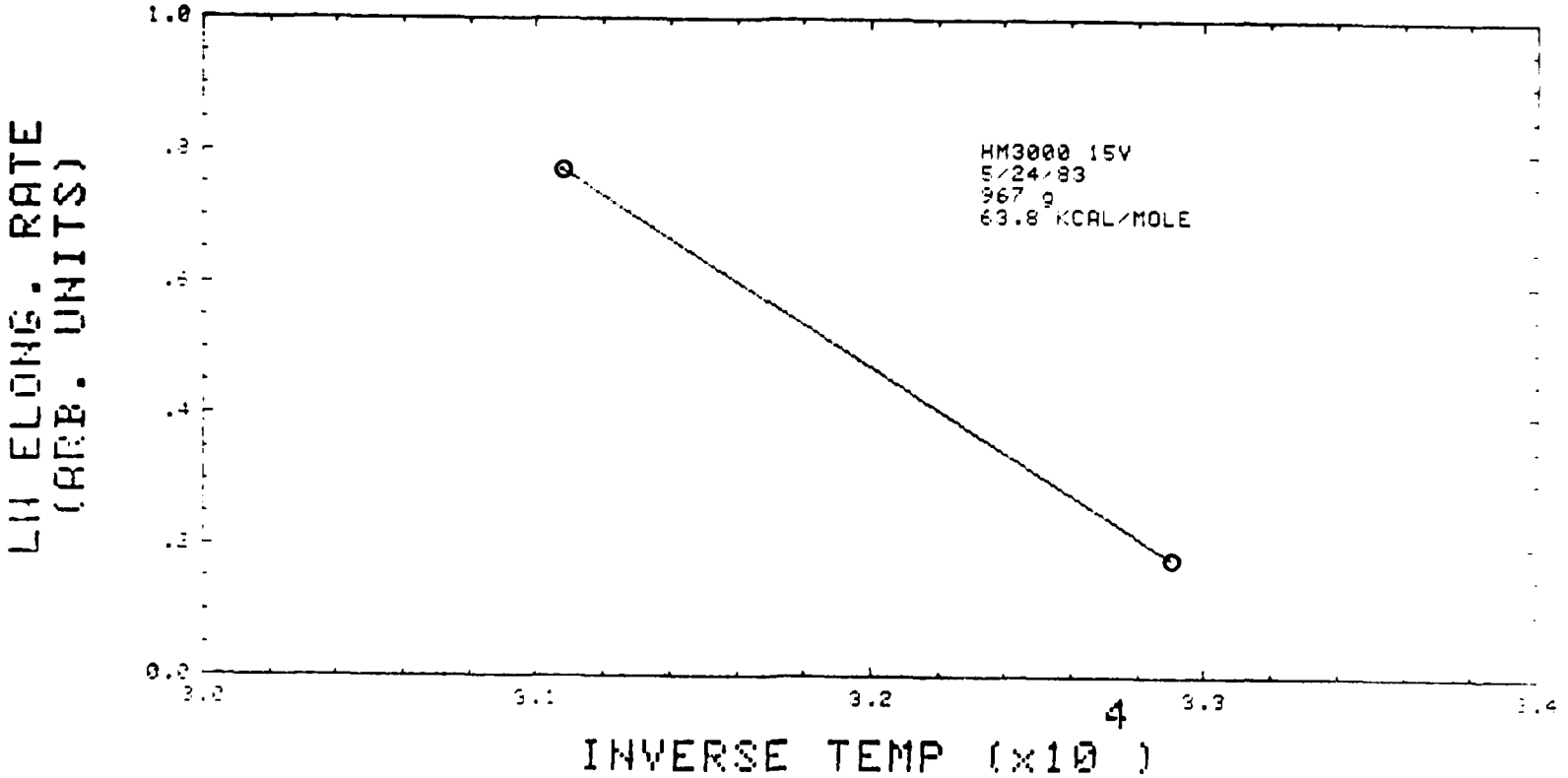

Fig.29 creep elongation rate vs. the inverse of absolute temperature

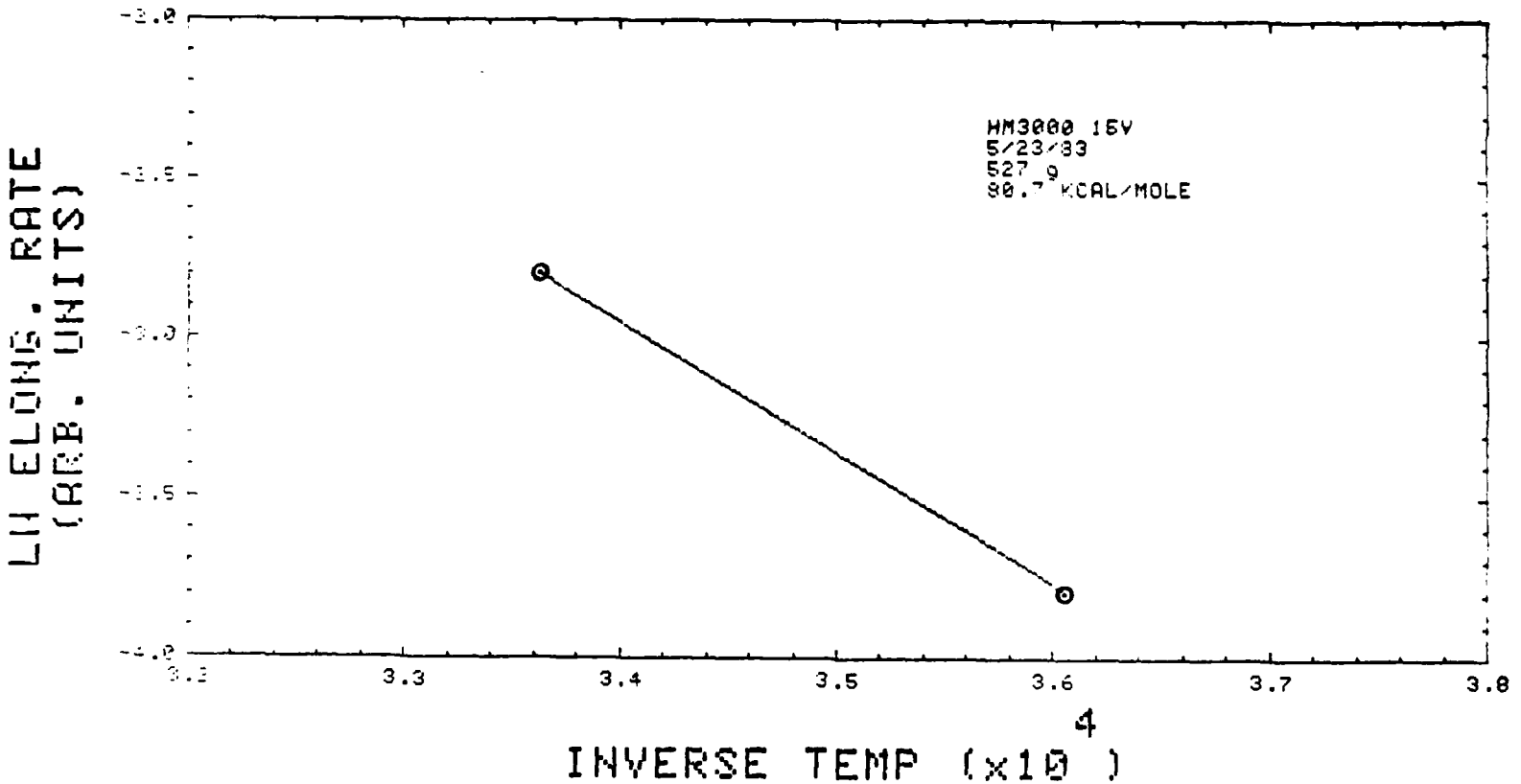

Fig.28 creep elongation rate vs. the inverse of absolute temperature

PROPERTY	HM- 3000	HM- 10,000
Density (lb/in^3)	0.067	0.066
Strength impreg. (ksi)	350	355
E_A (psi)	54×10^6	50×10^6
E_T (psi)	1.5×10^6	3.4×10^6
Diameter (μm)	7.2	7.5
α_A ($/^oF$)	*	1.39×10^{-6}
α_T ($/^oF$)	*	7.5×10^{-6}

Table 1 Conditioned properties of fibers used in this study at room temperature from their manufacturer's data

Property	Cool tar pitch 277CP - 15V
Density (gr/cc)	1.35
cooking value(%)	48.2
Benzene Insolubles(%)	12-18
Quinoline Insolubles(%)	4-8
Ash(%)	0.23

Table 2 Properties of 277CP-15V coal tar pitch matrix from their manufacturer's data

T (C)	n_1	n_2	n_3	n_4
2199.7	1.86	-	1.23	-
2380.0	1.92	-	1.50	-
2529.5	2.03	1.29	1.29	1.29
2680.2	2.16	1.30	1.53	1.66
2829.6	2.14	1.30	1.36	1.70

Table 3 Stress dependence values of HM 3000 fiber bundles

References

[1] B. Cohen, G. Sines,"Frabrication Stress and Crack Morphology of the Three-Dimensional Cylindrically Woven Carbon-Carbon Composites," UCLA-ENG-81-26, Sept. 1981, University of California Los Angeles.

[2] John J. Kibler, Kent W. Buesking, Jerry Rubinsky, "Exploratory Development of in-process Yarn Bundle Properties," Technical report AFWAL-TR-80-4096, 1980.

[3] Extended Abstracts of the 10th Biennial Conference on Carbon, 1971.

[4] J. Jortner, P. A. Tomlinson,"Application of Carbon-Carbon Composites to Rocket Nozzles," (ACORN)-Interim Report, AFML-TR-78-196, 1978.

[5] H. L. Cox,"The Elasticity and Strength of Paper and other Fibrous Materials," British Journal of Applied Physics, 3, 72-79, 1952.

[6] D. Hull,"An Introduction to Composite Materials," Cambridge University Press, 1981.

[7] L. Feldman,"High Temperature Creep of Carbon Yarn," 2nd annual Aerospace report, to be published.

Appendix

Calculate the Restraining Hydrostatic Pressures

Using the original billet model, one can solve for the interfacial pressure with no radial effect. With these informations one can find the hoop stress in the inner and outer most fiber,

$$\sigma_i = \frac{\left[P_{(0,1)} - P_{(1,2)}\right] R_i}{t_{f_i}}$$

and

$$\sigma_o = \frac{\left[P_{(58,59)} - P_{(59,60)}\right] R_o}{t_{f_o}}$$

where R_i , R_o , t_{f_i} , t_{f_o} are the inside and outside radius of the billet and fiber thickness at the inside and outside locations respectively.

The inside and outside circumferential strain are

$$\epsilon_i = \frac{\sigma_i}{(E_f)_{\hat{a}}}$$

and

$$\epsilon_o = \frac{\sigma_o}{(E_f)_{\hat{a}}}$$

The billet radius immediately after a rapid heat up is,

Appendix

Calculate the Restraining Hydrostatic Pressures

Using the original billet model, one can solve for the interfacial pressure with no radial effect. With these informations one can find the hoop stress in the inner and outer most fiber,

$$\sigma_i = \frac{\left[P_{(0,1)} - P_{(1,2)}\right] R_i}{t_{f_i}}$$

and

$$\sigma_o = \frac{\left[P_{(58,59)} - P_{(59,60)}\right] R_o}{t_{f_o}}$$

where R_i , R_o , t_{f_i} , t_{f_o} are the inside and outside radius of the billet and fiber thickness at the inside and outside locations respectively.

The inside and outside circumferential strain are

$$\epsilon_i = \frac{\sigma_i}{(E_f)_{\hat{a}}}$$

and

$$\epsilon_o = \frac{\sigma_o}{(E_f)_{\hat{a}}}$$

The billet radius immediately after a rapid heat up is,

$t_{f_i} = 0.035$ in

$t_{f_o} = 0.14$ in

$(E_f)_a = 25 \times 10^6$ psi at 5000 F

$\alpha_f = 1.39 \times 10^{-6}$/ F

$\Delta T = 4000$ F

$A_f = 9.43 \times 10^{-4}$ in^2

$A_{c_i} = 0.004$ in^2

$A_{c_o} = 0.007$ in^2

$\mu = 0.5$

Addendum I

Creep Parameter - The Linear Factor A

by

George Sines and Pascal Gotsis

One objective of the study was to determine the parameters in the creep equation for an impregnated graphite fiber bundle. The creep equation (VI-1) given on page 29 is

$$\frac{d\varepsilon}{dt} = A\sigma^{n}\exp(-\Delta H/RT)$$

Values of n are given in Table III and discussed on page 38. Values of ΔH were found from Figures 24 through 29 and discussed on page 36. The value for A requires special consideration.

In Figures 24 through 29, the ordinate is the natural logarithm of the displacement rate in millimeters/hr. The specimen is of uniform cross-section without a reduction in area in the gage length so the effective gage length must be estimated. It has been estimated from the temperature profile in the furnace that the effective gage length is 152 mm (6 inches). The data point for 2700°C on Figure 24 will be used for an estimate of A because it is on the best-fit straight line for the five data points and is a data point.

In obtaining a value of A, uncertainty exists or how to calculate the stress. Should the net fiber area be used on the gross area of the impregnated bundle? Both are meaningful.

Using the nominal net area of the bundle given by the supplier, 1.83×10^{-4} in^2, and the load of 273 grams (0.6018 lb) the stress is 3.18×10^3 psi. Using the mean value of n = 1.41, the mean value of 61.7 kcal/mol for the activation energy T = 2973°K, and a creep rate 4.76×10^{-3} hr^{-1}, we have $A = 1.76 \times 10^{-3}$ (where creep rate is in hr^{-1} and stress in psi). However, when we use the gross area of the impregnated bundle, which, admittedly, was somewhat irregular in diameter because of the pitch, taking an average diameter of 0.040 in, the stress is only 478 psi. Now we have an $A = 25.5 \times 10^{-3}$.

In our ongoing studies we will soon determine the effect of excess pitch on the creep rate. If it is negligible, then it would be appropriate to use the <u>in situ</u> cross-sectional area of the fiber bundle.

Addendum II

Comments on Activation Energy for Creep

by

George Sines

The creep tests were conducted on uni-directional specimens in which the PAN based fibers, "Hercules Magnamite" HM 3000, were graphitized by the supplier. The specimen was impregnated with coal tar pitch and carbonized according to the procedure outlined on pages 29-31. Thus, the state of the bundle would be representative of the first cycle of graphitization of the billet. The measured activation energy of 61.7 kcal/mol for the bundle in this state may not be representative of the bundle in later cycles of impregnation, carbonization, and graphitization, in which the matrix consist primarily of graphite. Fully graphitized specimens are being prepared to determine the effect of degree of graphitization of the matrix on the creep of the bundle.

Values measured by Feldman [II-I] on dry bundles of meso-pitch fibers of two kinds are 66 and 109 kcal/mol. His data for impregnated bundles were too scattered to yield an activation energy. An even wider range have been measured for polycrystalline carbon graphite, 60-239 kcal/mol [II-2].

Two activation energies may be active in the creep of graphites--that for the carbon-carbon bond of 85.3 kcal/mol and that for lattice diffusion of 163 kcal/mol [II-2]. Measurement of activation energy may also be distorted by the large transient creep that occurs in graphite.

Atom movement occurs in the graphitization of carbon as well as in creep. Two peaks have been observed at 100 and 200 kcal/mole in the graphitization of carbon [II-3]. They are thought to correspond to the same two mechanisms postulated for creep--carbon bond formation and lattice diffusion.

Pyrolytic graphite, because its atomic structure is similar to that of graphite fibers and to that of the matrix sheaf, could have a creep activation energy similar to that of a graphitized bundle. Values have been measured from 100 to 114 kcal/mol [II-4].

The creep behavior and the strength of multi-cycled, impregnated, graphitized bundles in cylindrically wound billets might be influenced by hot-working incurred by the thermal stresses during processing. Pyrolytic graphite has had its strength increased from an initial value of 26 to a final value of 87 ksi at 2200°C after it had been plastically deformed at 2750°C [II-4].

These uncertainties complicate the development of optimum processing to avoid failure of cylindrically wound billets because of the strong dependence of the analysis on the activation energy for creep. We hope to obtain better values on bundles processed in a manner simulating the billet processing.

References

II-1 L.A. Feldman, "Creep of Carbon Yarns and Composites at High Temperature," Extended Abstracts - 16th Biennial Conference on Carbon, San Diego, July 1983, 499, 500.

II-2 Leon Green, "Observations on the High Temperature Elastic and Inelastic Properties of Polycrystalline Graphites," Proc. Fourth Conference on Carbon, Pergamon 1960, 497-509.

III-3 Sanchi Mizushima, "Rate of Graphitization of Carbon," Proc. of the Fifth Conference on Carbon, Vol. 2, Macmillan, 1963, 439-447.

II-4 W.V. Kotlensky and H.E. Martens, "Mechanical Properties of Pyrolytic Graphite to 2800°C," Proc. Fifth Conference on Carbon, Vol. 2, Macmillan, 1963, 625-638.

AD-A144 751 THE EFFECTS OF RADIAL YARNS THREE-DIMENSIONALLY REINFORCED CARBON-CARBON..(U) CALIFORNIA UNIV LOS ANGELES SCHOOL OF ENGINEERING AND APPLIED..

2/2

UNCLASSIFIED D QUAN ET AL. 01 JUL 84 UCLA-ENG-84-22 F/G 11/4 NL

END

DATE FILMED

10-84

DTIC

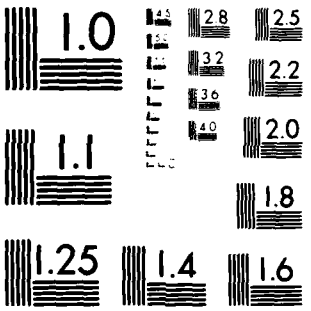

Addendum III

Considerations for Optimum Processing

by

George Sines and Pascal Gotsis

In our study of crack morphology of cylindrically wound, carbon-carbon billets, it appeared that the radial fibers had cracked free from the matrix [Text ref. 1]. There are reports that in some billets, when this debonding did not occur, the radial fibers fractured. In private communictaions [II-1], [II-2] it has been stated that the radials, even though they are debonded, may help prevent gross fracture of the billet. It is thought the high diametral expansion of the radials puts presure on the debonded interface so that the radials assume load through friction, thereby reducing the tension in the outer circumferential fibers. This has never been confirmed. We plan to test this hypothesis in our proposed experimental program.

To give a qualitative understanding of the shape of the optimum time-temperature heating path to avoid radial fiber-bond failure or fiber fracture, we treat a simplified worse case. Consider a cartesian lay-up in which the fibers under consideration are a minority so that their stress does not appreciably retard thermal strain of the composite in their longitudinal direction. To avoid fracture of the fibers or their debonding, the difference between the thermal strain of the fibers and the composite must be less than the critical elastic strain to cause failure plus the creep strain of the fibers.

$$(\alpha_m - \alpha_f)T(t) \leq \frac{\sigma_{crit}}{E_F} + \int_{(o)}^{(t)} \dot{\varepsilon}\, dt$$

This equation is solved in the text on page 23 and the symbols are defined there. (α_m is the transverse coefficient of the composite in which direction there are very few fibers)

$$t = \left[(\alpha_m - \alpha_f)/A\ \sigma_{crit}^n\right] \int_{T_o}^{T} \exp\left[\Delta H/RT\right] dT$$

The integral does not exist in closed form but had to be evaluated numerically by the IMSL subroutine library of the IBM 3033 computer. the initial heating to T_o without creep which causes a fiber stress of σ_{crit}, which has some margin of safety, can follow any path. It is at this temperature the calculated path starts.

The material parameters used in the calculation are:

$$\alpha_m = 5.45 \times 10^{-6}\ (°C)^{-1}$$

$$\alpha_f = 7.72 \times 10^{-7}\ (°C)^{-1}$$

$$E = 16.2 \times 10^{6}\ \text{psi}$$

$$n = 1.41$$

$$A = 1.81 \times 10^{-3}\ (\text{stress in psi, creep rate in } hr^{-1})$$

A was determined for the best fit to the data of Figure 24. The stress was based on net fiber area.

In Figure III-1 the path is given for σ_{crit} = 130 ksi and T_o = 1715°K. To avoid failure, one hour must be taken to raise the temperature the first increment of 200°K. After 1.1 hours, the temperature can be raised at a very rapid rate, not needing more than an additional 0.02 hr to reach any temperature of interest for graphitization.

In Figure III-2 for σ_{crit} = 100 ksi, the initial temperature is 1319°K, and 2.2 x 10^2 hr is needed to raise the temperature 200°K without failure. However, only an additional 15 hr are needed to raise the temperature an additional 1500°K.

In Figure III-3 for σ_{crit} = 140°K, the total time, after reaching a T_o = 1847°K, is less than 0.4 hr to reach 3000°K.

These calculations for cartesian lay-up are very conservative when compared to the behavior of a cylindrical lay-up in which the transverse (radial) strain is greatly constrained by the circumferential fibers. However, they do illustrate the extreme sensitvity of the time-temperature path to the failure strength of the radial fibers. They also show the need to slowly raise the temperature in the initial period after T_o has been reached.

These calculations are applicable to cartesian lay-up. The constraint of the transverse fibers would have to modify the thermal strain

$k\,\sigma_{crit}(\alpha_m - \alpha_f)$ in the initial equation.

where the constraint factor k would have to be found from micromechanics. In this simple illustration the material properties were considered to be constant. More accurate analysis would have them dependent on temperature.

III-1 Private Communication - Julius Jortner, 1982

III-2 Private Communication - Steven Evangelides, 1982

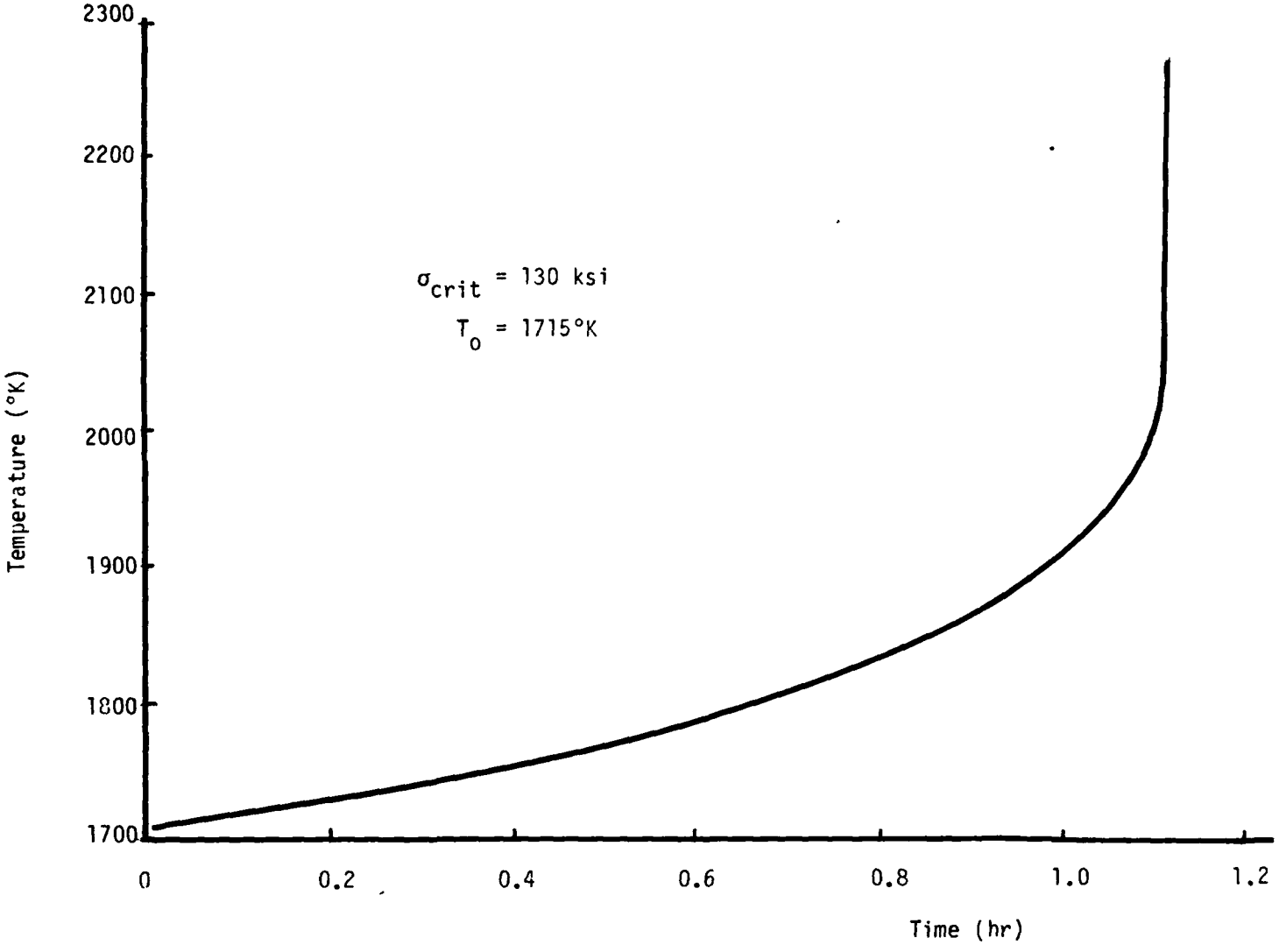
2300
2200
2100
2000
1900
1800
1700
Temperature (°K)
σ_{crit} = 130 ksi
T_o = 1715°K
0
0.2
0.4
0.6
0.8
1.0
1.2
Time (hr)

Figure III-1

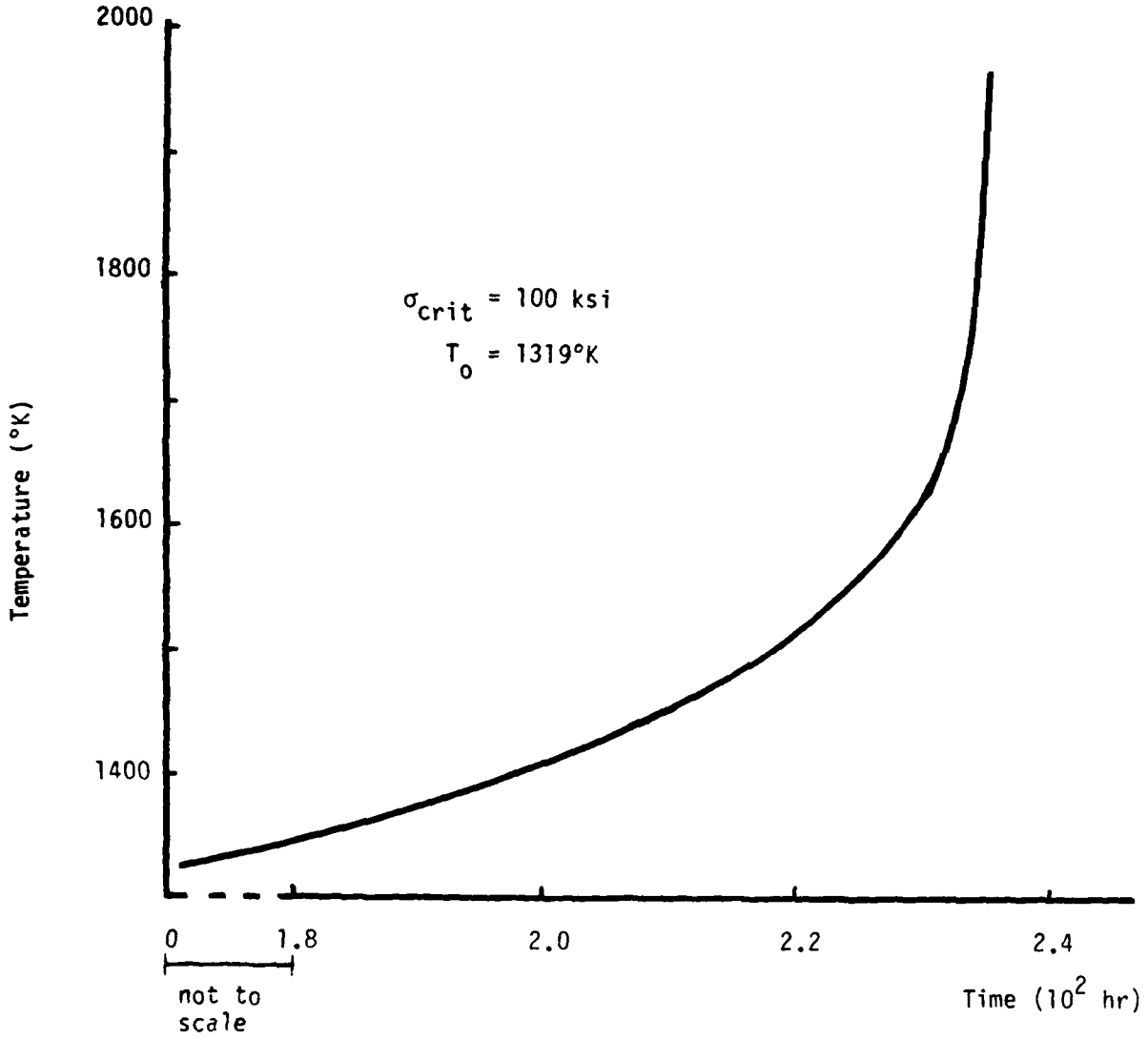
2000
1800
1600
1400
Temperature (°K)
σ_{crit} = 100 ksi
T_o = 1319°K
0
1.8
2.0
2.2
2.4
not to scale
Time (10^2 hr)

Figure III-2

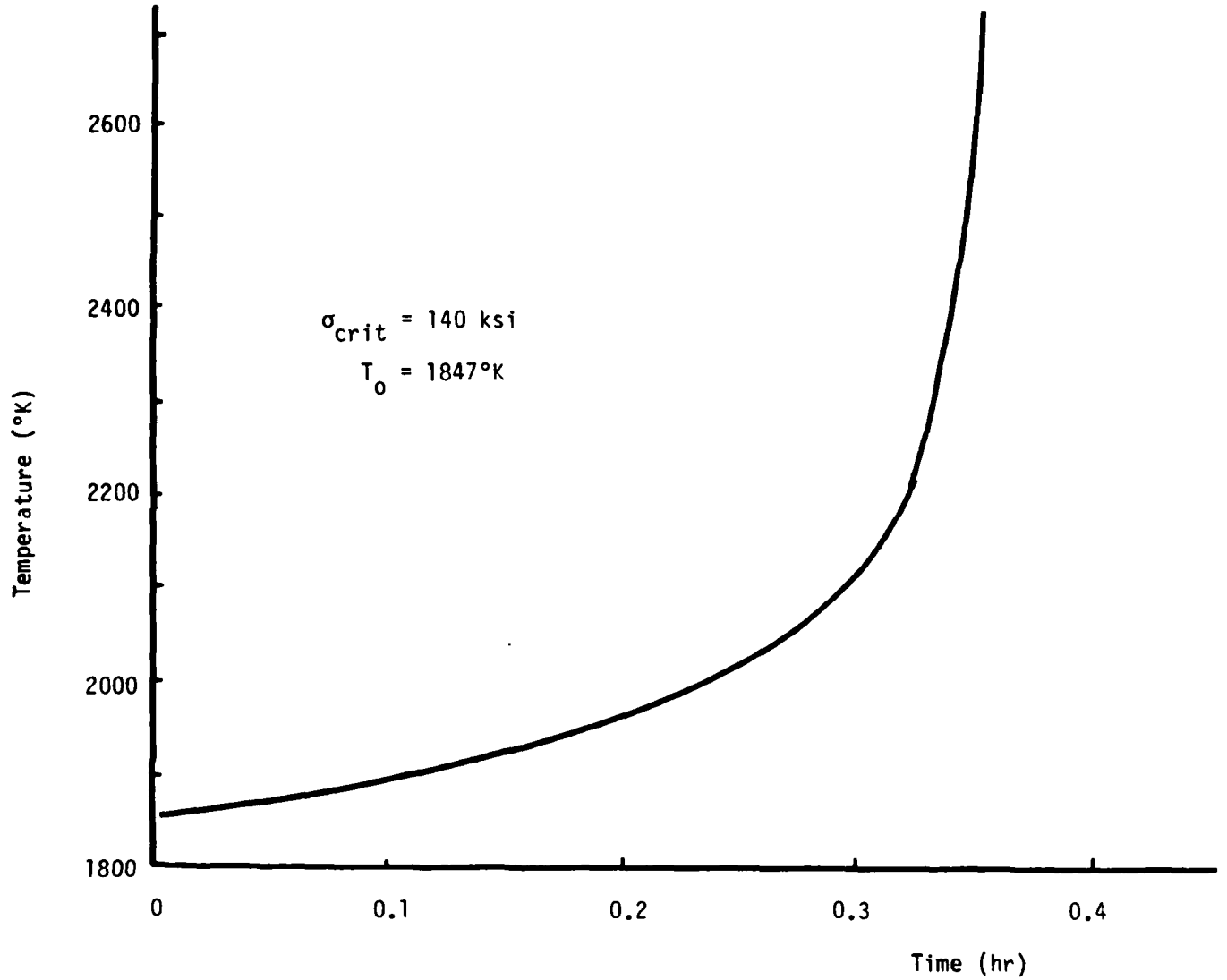
2600
2400
2200
2000
1800
Temperature (°K)
σ_{crit} = 140 ksi
T_o = 1847°K
0
0.1
0.2
0.3
0.4
Time (hr)

Figure III-3

ADDENDUM IV

Stresses in the Radial Bundles - Further Considerations

by

George Sines

The model used for the first-order approximation compared the axial strains in the circumferential bundles at the inner and outer diameters of the billet to the average axial strain of a radial bundle attached to these extreme circumferential bundles. (Eq. I-8, page 9) It was demonstrated that the stress in the radial bundles exceeds that in the circumferential bundles when the billet is heated.

This model neglected the local interaction of the radial bundles with the thermal strain of the composite. Julius Jortner recently made a second-order approximation* which gives

$$\frac{{}^{B}\bar{\varepsilon}_{r}}{{}^{B}\varepsilon_{\theta}^{*}} \simeq \frac{{}^{c}\varepsilon_{\theta}^{*}\ \dfrac{(R_o + R_i)}{(R_o - R_i)} + ({}^{c}\alpha_{\theta} - {}^{B}\alpha)\Delta T}{{}^{c}\varepsilon_{\theta}^{*} + ({}^{c}\alpha_{\theta} - {}^{B}\alpha)\Delta T}$$

Where ${}^{B}\bar{\varepsilon}_{r}$ average axial mechanical strain in a radial bundle.

${}^{B}\varepsilon_{\theta}^{*}$ axial tensile mechanical strain in a circumferential bundle at the outer radius R_o. (It is assumed to be approximately equal in magnitute to the compressive strain in the circumferential bundle at the inner radius R_i).

${}^{c}\varepsilon_{\theta}^{*}$ mechanical circumferential strain in the composite at R_o.

${}^{c}\alpha_{\theta}$ coefficient of thermal expansion of the composite in the circumferential direction.

---

* To appear in a forthcoming report by Jortner Research to the ONR. (L.H. Peebles, Jr., ONR monitor.)

$^{B}\alpha$ axial coefficient of thermal expansion of the bundle.

Notice that this analysis also predicts that the strain (stress) in the radial bundles is always higher than the peak strain (stress) in the circumferential bundles.

Both models are limited to giving the average of the axial mechanical strain in the radial bundles; it will be seen that the peak strain in the radial bundles will be even higher: The radial composite stress (or strain) which occurs upon heating is compressive and it is zero at the outer and at the inner radii and has a roughly parabolic shape with the peak near the middle of the radial thickness (Reference 1, Figure 23). Shear interaction of the radial bundles with this compressive composite strain would decrease the axial tensile strain in the bundles in the middle and would therefore increase it near the outer and inner radii in order to maintain the same average strain. Thus the axial tensile stress in the radial bundles would be higher near the outer and inner radii and higher than the average predicted by both of the above analyses. (Jortner considers the above in a quantitative way in the draft of his report in preparation.)

Many billets have a layered structure where the number of radial fibers is increased at the outer radius in an attempt to make the radial bundle density more constant. Neither analyses considers this effect or the coincident effect of termination of some fibers at the layer interfaces.

ONR DISTRIBUTION (CARBON-CARBON)

ORGANIZATION	LASTNAME	FIRSTNAME	CITY	STATE	ZIPCODE
ACUREX/AEROTHERM	Carlson	D. L.	Mountain View	CA	94042
ACUREX/AEROTHERM	Zimmer	J. E.	Mountain View	CA	94042
AEROJET ELECTROSYSTEMS	Buch	J. D.	Azusa	CA	91702
AEROJET STRATEGIC PROPULSION COMPANY	Davis	H. O.	Sacramento	CA	95813
AEROJET STRATEGIC PROPULSION COMPANY	Marchol	P.	Sacramento	CA	95813
AERONUTRONIC FORD	Pope	J.	Newport Beach	CA	92663
AEROSPACE CORPORATION	Baker	R. L.	Los Angeles	CA	90009
AEROSPACE CORPORATION	Chase	A. B.	Los Angeles	CA	90009
AEROSPACE CORPORATION	Evangelides	J. S.	Los Angeles	CA	90009
AEROSPACE CORPORATION	Feldman	L.	Los Angeles	CA	90009
AEROSPACE CORPORATION	Meyer	Robert A.	Los Angeles	CA	90009
AEROSPACE CORPORATION	Robinson	E. Y.	Los Angeles	CA	90009
AEROSPACE CORPORATION	Rubin	L.	Los Angeles	CA	90009
AEROSPACE CORPORATION	White	J. L.	Los Angeles	CA	90009
AFOSR/NC	Ulrich	D. R.	Bolling AFB	DC	20332
AFWAL/MLBC	Abrams	Frances	Wright-Patterson AFB	OH	45433
AFWAL/MLBC	Schmidt	D.	Wright-Patterson AFB	OH	45433
AFWAL/MLBC	Theibert	L. Scott	Wright-Patterson AFB	OH	45433
AFWAL/MLBE	Craig	R. E.	Wright-Patterson AFB	OH	45433
AFWAL/MLBL	Kessler	W. C.	Wright-Patterson AFB	OH	45433
AFWAL/MLBM	Drzal	L. T.	Wright-Patterson AFB	OH	45433
AFWAL/MLBM	Pagano	N. J.	Wright-Patterson AFB	OH	45433
AFWAL/MLLM	Graham	H. C.	Wright-Patterson AFB	OH	45433
AFWAL/MLLM	Kerans	R.	Wright-Patterson AFB	OH	45433
AFWAL/MS	Tallan	N. M.	Wright-Patterson AFB	OH	45433
AFWL/NTY	**********		Kirtland AFB	NM	87117
AIR FORCE ROCKET PROPULSION LABORATORY	De Hoff	Brian	Edwards AFB	CA	93523
AIR FORCE ROCKET PROPULSION LABORATORY	Tepe	L.	Edwards AFB	CA	93523
ARMY MATERIALS & MECHANICS RES. CENTER	Dignam	J.	Watertown	MA	02172
ARMY RESEARCH OFFICE	Meyer	George	Research Triangle Pk	NC	27709
ATLANTIC RESEARCH CORPORATION	Baetz	J.	Alexandria	VA	22314
ATLANTIC RESEARCH CORPORATION	Frankle	R. S.	Alexandria	VA	22314
AVCO Corporation	Laskaris	T.	Lowell	MA	01851
AVCO Corporation	Rolincik	P.	Wilmington	MA	01887
AVCO Systems Division	Taverna	Art	Wilmington	MA	01887
B.F. GOODRICH R&D CENTER	Stover	E.	Brecksville	OH	44191
BATTELLE COLUMBUS LABORATORIES	Jelinek	Frank J.	Columbus	Ohio	43201
CALIFORNIA RESEARCH & TECHNOLOGY, INC.	Kreyenhagen	K. N.	Chatsworth	CA	91311
DEFENSE NUCLEAR AGENCY	Kohler	B.	Washington	DC	20305
DEFENSE TECHNICAL INFORMATION CENTER	**********		Alexandria	VA	22314
DEPARTMENT OF THE NAVY	Crone	J.	Washington	DC	20360
EFFECTS TECHNOLOGY, INC.	Adler	M.	Santa Barbara	CA	93105
EFFECTS TECHNOLOGY, INC.	Graham	M.	Santa Barbara	CA	93105
EIXON ENTERPRISES, INC.	Riggs	D.	Fountain Inn	SC	29644
FIBER MATERIALS, INC.	Lander	L. L.	Biddeford	ME	04005
FIBER MATERIALS, INC.	McAllister	L.	Biddeford	ME	04005
GA Technologies	Engle	Glen B.	San Diego	CA	92138
GENERAL ELECTRIC COMPANY	Franke	Robert	Cincinnati	OH	45215
GENERAL ELECTRIC COMPANY	Hall	Kenneth J.	Philadelphia	PA	19101
GENERAL ELECTRIC SPACE DIVISION -RSO	Gebhardt	J.	Philadelphia	PA	19101
HAVEG	Pegg	R.	Santa Fe Springs	CA	90670
HERCULES CORPORATION	Christensen	P.	Magna	UT	84044

ONR DISTRIBUTION (CARBON-CARBON)

ORGANIZATION	LASTNAME	FIRSTNAME	CITY	STATE	ZIPCODE
HITCO	Dyson	L.	Gardena	CA	90249
IIT Research Institute	Larsen	D. C.	Chicago	Illinois	60616
JET PROPULSION LABORATORY	Kimmel	M.	Pasadena	CA	91103
JORTNER RESEARCH & ENGINEERING, INC.	Jortner	Julius	Costa Mesa	CA	92628
KAISER	Fischer	M.	San Leandro	CA	94577
LAWRENCE LIVERMORE LABORATORIES	Maimoni	A.	Livermore	CA	94550
LOCKHEED MISSILES & SPACE COMPANY, INC.	Pinoli	Pat C.	Palo Alto	CA	94304
LOCKHEED MISSILES AND SPACE COMPANY	Osaka	M.	Sunnyvale	CA	94088
MARTIN MARIETTA AEROSPACE	Koo	F. M.	Orlando	FL	32855
MASSACHUSETTS INSTITUTE OF TECHNOLOGY	Uhlman	D. R.	Cambridge	MA	02139
MATERIALS SCIENCES CORPORATION	Kibler	J. J.	Springhouse	PA	19477
MATERIALS SCIENCES CORPORATION	Rosen	B. Walter	Springhouse	PA	19477
MCDONNELL DOUGLAS ASTRONAUTICS CO.	Greszczuk	L. B.	Huntington Beach	CA	92647
MCDONNELL DOUGLAS ASTRONAUTICS CO.	Penton	A. P.	Huntington Beach	CA	92647
MCDONNELL DOUGLAS RESEARCH LABORATORY	Holman	M.	St. Louis	MO	63166
NASA	Bersch	Charles F.	Washington	DC	20546
NASA Langley	Houston	R. J.	Langley	VA	23665
NASA Langley	Rummler	D.	Langley	VA	23665
NASA Langley	Sawyer	J. W.	Langley	VA	23665
NASA Marshall Space Flight Center	Powers	B.	Huntsville	AL	35812
NAVAL RESEARCH LABORATORY	**********		Washington	DC	20375
NAVAL SEA SYSTEMS COMMAND	Kinna	M.	Washington	DC	20302
NAVAL WEAPONS CENTER	Jeter	Edward	China Lake	CA	93555
NSWC/WOL	Koubek	F. J.	Silver Spring	MD	20910
NSWC/WOL	Rowe	Charles R.	Silver Spring	MD	20910
OFFICE OF NAVAL RESEARCH	**********		Pasadena	CA	91106
OFFICE OF NAVAL RESEARCH	Diness	A. M.	Arlington	VA	22217
OFFICE OF NAVAL RESEARCH	Kushner	A. S.	Arlington	VA	22217
OFFICE OF NAVAL RESEARCH	Peebles	L. H.	Arlington	VA	22217
OSD/DDR&E	Persh	J.	Washington	DC	20301
PDA Engineering	Crose	J. G.	Santa Ana	CA	92705
PDA Engineering	Mack	T. E.	Santa Ana	CA	92705
PDA Engineering	Stanton	E. L.	Santa Ana	CA	92705
PICATINNY ARSENAL	Anazione	A.	Dover	NJ	07801
PRATT & WHITNEY AIRCRAFT	Miller	Robert L.	West Palm Beach	FL	33402
PRATT & WHITNEY AIRCRAFT	Schmid	Tom	West Palm Beach	FL	33402
PURDUE UNIVERSITY	Sun	C. T.	West Lafayette	IN	47907
PURDUE UNIVERSITY	Taylor	R. E.	West Lafayette	Indiana	47906
RENSSELAER POLYTECHNIC INSTITUTE	Diefendorf	R. J.	Troy	NY	12181
ROCKETDYNE DIVISION, ROCKWELL INTERNTL	Hawkinson	E. L.	Canoga Park	CA	91304
SAMSO/MNNR	Bailey	D.	Norton AFB	CA	92409
SAMSO/MNNR	Brocato	T.	Norton AFB	CA	92409
SANDIA LABORATORIES	Northrup	D.	Albuquerque	NM	87185
SCIENCE APPLICATIONS, INC.	Eitman	D.	Irvine	CA	92715
SCIENCE APPLICATIONS, INC.	Loomis	Willard	Irvine	CA	92715
SOUTHERN RESEARCH INSTITUTE	Koenig	John	Birmingham	AL	35205
SOUTHERN RESEARCH INSTITUTE	Pears	C.	Birmingham	AL	35205
SOUTHERN RESEARCH INSTITUTE	Starrett	H. Stuart	Birmingham	AL	35205
SOUTHWEST RESEARCH INSTITUTE	Lankford	J.	San Antonio	TX	78284
SOUTHWEST RESEARCH INSTITUTE	Robinson	Craig	San Antonio	TX	78282
STACKPOLE FIBERS COMPANY, INC.	Fleming	G.	Lowell	MA	01852
STRATEGIC SYSTEMS PROJECT OFFICE (PM-1)	Kincaid	J.	Washington	DC	20376

ONR DISTRIBUTION (CARBON-CARBON)

ORGANIZATION	LASTNAME	FIRSTNAME	CITY	STATE	ZIPCODE
STRATEGIC SYSTEMS PROJECT OFFICE (PM-1)	Weinger	S.	Washington	DC	20376
SUPERTEMP CENTER	Leeds	Don	Santa Fe Springs	CA	90670
SYSTEMS, SCIENCE AND SOFTWARE	Gurtman	G.	La Jolla	CA	92037
THIOKOL	Broman	G.	Brigham City	UT	84302
TRW Systems	Kotlensky	Wm.	San Bernardino	CA	92402
U.S. ENERGY RESEARCH DIV. ADMINISTRATION	Littman	A.	Washington	DC	20331
UNION CARBIDE CORPORATION	Bowman	J.	Cleveland	OH	44101
UNION CARBIDE CORPORATION	Taylor	A.	Oak Ridge	TN	37839
UNITED TECHNOLOGIES RESEARCH CENTER	Gallaso	F.	Hartford	CT	06100
UNITED TECHNOLOGIES-CSD	Ellis	Russ	Sunnyvale	CA	94088
UNIVERSITY OF CALIFORNIA	Batdorf	S. B.	Los Angeles	CA	90024
UNIVERSITY OF CALIFORNIA	Sines	George	Los Angeles	CA	90024
UNIVERSITY OF WASHINGTON	Fischbach	D.	Seattle	WA	98195
UNIVERSITY OF WYOMING	Adams	D. F.	Laramie	WY	82071
VIRGINIA POLYTECHNIC INSTITUTE	Hasselman	D. P. H.	Blacksburg	VA	24061
VIRGINIA POLYTECHNIC INSTITUTE	Jones	Robert M.	Blacksburg	VA	24061
VOUGHT CORPORATION	Volk	H.	Dallas	TX	75211
WILLIAMS INTERNATIONAL	Cruzen	Scott	Walled Lake	MI	48088


ATE
LME